Leishmania donovani Aurora kinase: a promising therapeutic target against visceral leishmaniasis

Rudra Chhajer, Anirban Bhattacharyya, Nicky Didwania, Md Shadab, Nirupam Das, Partha Palit, Tushar Vaidya, Nahid Ali

PII: S0304-4165(16)30210-0
DOI: doi: 10.1016/j.bbagen.2016.06.005
Reference: BBAGEN 28517

To appear in: *BBA - General Subjects*

Received date: 8 January 2016
Revised date: 2 June 2016
Accepted date: 6 June 2016

Please cite this article as: Rudra Chhajer, Anirban Bhattacharyya, Nicky Didwania, Md Shadab, Nirupam Das, Partha Palit, Tushar Vaidya, Nahid Ali, Leishmania donovani Aurora kinase: a promising therapeutic target against visceral leishmaniasis, *BBA - General Subjects* (2016), doi: 10.1016/j.bbagen.2016.06.005

Title: Leishmania donovani Aurora kinase: a promising therapeutic target against visceral leishmaniasis

Authors: Rudra Chhajer[1], Anirban Bhattacharyya[1], Nicky Didwania[1], Md Shadab[1], Nirupam Das[2], Partha Palit[2], Tushar Vaidya[3] and Nahid Ali[1#]

[1]Infectious Diseases and Immunology Division, Council of Scientific and Industrial Research (CSIR)-Indian Institute of Chemical Biology, 4 Raja S. C. Mullick Road, Jadavpur, Kolkata 700032, West Bengal, India.

[2] Assam University, Silchar (A Central University), Dept. of Pharmaceutical Science, Division of Drug Discovery Lab, Silchar -788011, Assam, India

[3] Council of Scientific and Industrial Research (CSIR)- Centre for Cellular and Molecular Biology, Uppal Road, Habshiguda, Hyderabad 500007, Telangana, India.

Running title: Aurora Kinases Are Important for Leishmania Cytokinesis

[#]**To whom correspondence should be addressed:** Prof. Nahid Ali, Infectious Diseases and Immunology Division, Council of Scientific and Industrial Research (CSIR)-Indian Institute of Chemical Biology, 4 Raja S. C. Mullick Road, Jadavpur, Kolkata 700032, West Bengal, India.

Tel: 91-33-2499-5757 / **Fax:** 91-33-2473-0284/5197/ **E-mail:** nali@iicb.res.in

Keywords: Aurora kinase; cytokinesis; hesperadin; therapeutic target; cell-cycle; *Leishmania donovani*

ABSTRACT

BACKGROUND-Aurora kinases are key mitotic kinases executing multiple aspects of eukaryotic cell-division. The apicomplexan homologs being essential for survival, suggest that the *Leishmania* homolog, annotated Ld*AIRK*, may be equally important.

METHODS-Bioinformatics, stage-specific immunofluorescence microscopy, immunoblotting, RT-PCR, molecular docking, in-vitro kinase assay, anti-leishmanial activity assays, flow cytometry, fluorescence microscopy.

RESULTS-Ld*AIRK* expression is seen to vary as the cell-cycle progresses from G1 through S and finally G2M and cytokinesis. Kinetic studies demonstrate their enzymatic activity exhibiting a Km and Vmax of 6.12µM and 82.9pmoles.min^{-1}mg^{-1} respectively against ATP using recombinant *Leishmania donovani* H3, its physiological substrate. Due to the failure of Ld*AIRK*-/+ knock-out parasites to survive, we adopted a chemical knock-down approach. Based on the conservation of key active site residues, three mammalian Aurora kinase inhibitors were investigated to evaluate their potential as inhibitors of Ld*AIRK* activity. Interestingly, the cell-cycle progressed unhindered, despite treatment with GSK-1070916 or Barasertib, inhibitors with greater potencies for the ATP-binding pocket compared to Hesperadin, which at nanomolar concentrations, severely compromised viability at IC50s 105.9 and 36.4nM for promastigotes and amastigotes, respectively. Cell-cycle and morphological studies implicated their role in both mitosis and cytokinesis.

CONCLUSION-We identified an Aurora kinase homolog in *L. donovani* implicated in cell-cycle progression, whose inhibition led to aberrant changes in cell-cycle progression and reduced viability.

GENERAL SIGNIFICANCE- Human homologs being actively pursued drug targets and the observations with Ld*AIRK* in both promastigotes and amastigotes suggest their potential as therapeutic-targets. Importantly, our results encourage the exploration of other proteins identified herein as potential novel drug targets.

1. Introduction

During its life cycle, *Leishmania* alternates between the extracellular promastigote form and the intracellular amastigote form triggered by variations in pH, temperature and other biomolecules within the macrophage. A downstream signal transduction process thus induced brings about changes necessary for its survival in the new environment and pathogenicity. Since trypanosomatids transcribe most genes in large polycistronic units, signaling cascades here, possibly function by post-transcriptional regulation. Phosphoproteome analysis by LC-MS/MS and comparative bio-informatics reveals that the overall phosphorylation pattern in *Leishmania* and related trypanosomatids change substantially during this differentiation [1]. Some critical developmentally and differentially regulated genes have been identified in *Leishmania donovani* and *Leishmania infantum* by microarray technology [2,3]. Furthermore, many kinases with unknown functions, showing no apparent affinity to any known group, 63% being absent in *Leishmania major, Trypanosoma brucei or Trypanosoma cruzi* have been identified [4]. Kinase dysregulation is often the cause or end result of many diseases. As such numerous inhibitors have been developed against them [5]. Subsequently, the *L. donovani* kinome represents an appealing target for potential anti-leishmanials, their well-understood active sites facilitating the design of small molecules. A few instances of favourable outcomes include the inhibition of cGMP-dependent protein kinase (PKG) against *Eimeria* and *Toxoplasma*; and purvalanol B, a purine-based CDK inhibitor with unexpected targets in numerous protozoan parasites [6].

Several evolutionarily conserved serine/ threonine kinases have been implicated in eukaryotic cell-cycle regulation, some of which include the cyclin-dependent kinases, Polo-like kinases, Nima-related kinases and Aurora kinases [7]. However, these mitotic kinases demonstrate considerable variations in the organization and regulation of the cell-cycle, lending hope that specific inhibition may be achieved against the lower eukaryotes. Compared with other eukaryotes, few conserved mitotic proteins involved in the G2/M phase have been identified in *T. brucei*. These include cyclin homologs (CYC6 and CycB2), cdc2-related kinase (CRK3), Aurora kinase homologue (TbAUK1) and homologues of the anaphase promoting complex/ cyclosome (APC1 and CDC27) [7]. In fact, no homologues of conventional centromeric or kinetochore proteins involved in mitosis have yet been identified [8]. Given their demonstrated essential roles in numerous organisms, these enzymes represent potential drug targets for antiparasitic intervention [9-12].

Among the most important and well studied mitotic serine/threonine kinases, are the Aurora kinases. They consist of one member in *Saccharomyces cerevisiae* (Ipl1), two in *Caenorhabditis elegans* (AIR-1, AIR-2), two in *Drosophila melanogaster* (Aurora-A, IAL) and three members in *Homo sapiens* (Aurora-A, Aurora-B, Aurora C and one pseudogene). Recently, three members in *T. brucei* (TbAUK1, 2, 3), three in *Plasmodium falciparum* (Pfark1, 2, 3) and one in *L. major* (Lmairk) have been identified [13-15]. In yeast (*Saccharomyces cerevisiae* and *Saccharomyces pombe*), mycetozoa (*Dictyostelium discoideum*), primitive deuterostome (starfish, ascidian and

urchin), etc. the only Aurora kinase shows the localization and function of both Aurora A and B of higher species [16].

The crucial role played by Aurora kinases acquires significance due to their involvement with the interphase centrosomes, generation of mitotic spindles and chromosomal ploidy. Moreover, their up-regulation in several cancer types has led to the development of several Aurora kinase agonists [17]. Danusertib, a pan-Aurora kinase inhibitor, was the first to enter phase I and II trials [11,17]. Recent studies, have demonstrated its activity against *T. brucei, L. major* and *P. falciparum* too [11,18]. Aurora kinase inhibition being naturally selective towards cells depleted of certain mitotic checkpoint proteins and a dysfunctional p53 instead of healthy cells, promises fewer adverse effects [19].

Consistent with their localizations, Aurora A (the polar auroras) regulate spindle assembly, and Aurora B (the equatorial auroras) control chromosome segregation and cytokinesis initiation as part of the chromosomal passenger complex (CPC). The CPC is a complex of four proteins-INCENP, Borealin/Dasra, Survivin and Aurora B kinase in mammals that are replaced by Sli15p, Bir1p, Nbl1p and IpL1 respectively in budding yeast [20,21]. Additionally, mammalian Aurora A and its homologue in *Chlamydomonas* are involved in cilia and flagellar disassembly too [22,23]. In *P. falciparum*, failed attempts to disrupt the pfark-1, pfark-2 or pfark-3 loci suggest the non-redundant and essential roles they play here [17]. In *T. brucei*, RNAi silencing of TbAUK1, -2 and -3 individually proved the essentiality of the multitasking TbAUK1 homolog over the other two which alone couples mitosis, kinetoplast replication and cytokinesis. Furthermore, the disappearance of mitotic spindles upon TbAUK1 deletion accompanied by its localization to the middle of the apparent spindle pole body during metaphase and late anaphase highlights its similarity to the Aurora B like kinases [24,25]. Dominant negative overexpression of a TbAUK1 mutant, in the bloodstream parasites, adversely affected the formation of mitotic spindles, chromosomal segregation as well as cytokinesis. In procyclics, cytokinesis proceeded even in the presence of a blocked mitosis, depending mainly on the basal body separation, unlike the bloodstream form where the completion of mitosis was prerequisite for cytokinetic initiation [24]. Interestingly, the typical cellular architecture was also lost, unlike the procyclic form that retained its normal spindle-like shape. However, genomic DNA synthesis and organeller replications persisted instead of just doubling (as observed in the similarly treated procyclics), thus producing giant polyploid cells with several kinetoplasts, basal bodies, nucleoli, and flagella. Moreover, TbAUK1 inhibition, in the bloodstream form adversely affects infection in mice, implying its role in virulence too.

In the present work, we use computational analysis to mine the genomic and proteomic databases of *Leishmania* and related protozoan parasites based on a primary literature survey of essential protozoan pathways. Open-access resources comprising databases for kinetoplastid parasites like TriTrypDB, geneDB and TDRtargets that facilitate drug target prioritization were used. Upon screening 60 candidate proteins, we proceeded with the initial characterization of the

most promising target revealed. This was a putative Aurora-like kinase, annotated Ldairk based on the nomenclature of Lmairk from *L. major*.

The characterizations in the parasitic protozoa like *T. brucei* were attained by RNAi-mediated knockdown and subsequent functional studies. However, the lack of such machinery in *L. donovani*, much like *P. falciparum*, makes gene knock-outs the gold standard for functional genetic studies. It is pertinent here to say, that despite many attempts, the gene knockout parasites failed to survive, which although precluded further studies, it strengthened our hypothesis of the importance of Ld*AIRK* in the parasites biology (Supplementary Figure 5). Hence, chemical knock down studies were adopted to evaluate their functional relevance.

In this study, we report the identification, characterization and functional ability of *L .donovani AIRK* to ascertain its viability in drug development. The *L. donovani* gene has been cloned, expressed and purified for *in vitro* studies and the expression patterns of the protein at both transcriptional and translational levels, examined at different phases of the promastigote cell-cycle. Unlike in *T. brucei*, Ld*AIRK* remains extra nuclear throughout the cell-cycle. Temporal shifts in positioning from the cytoplasm to the nuclear periphery and ultimately to the spindle poles, as the cell progresses through early mitosis to post-mitosis, demonstrates its similarity to the multi-tasking *S. cerevisiae* homolog. Inhibition of *Leishmania* promastigotes by Hesperadin, a mammalian Aurora kinase B inhibitor, results in cells concentrating at the G2/M phase (representing 2N DNA content) and even beyond, implicating a possible role in cytokinesis and cell-cycle progression. The chromatin synthesis continues despite the segregation block on nuclear material and cytokinesis. Inhibitions with Barasertib or GSK-1070916 that have greater potencies and target other kinases too were only slightly inhibitory to *L. donovani* growth and failed to exhibit such a pronounced effect, highlighting similarity to the mammalian Aurora kinase B homolog. Although showing high resemblance ~ 79% to the TbAUK1 homolog, the *L. donovani* promastigotes fail to retain their cellular and cytoskeletal integrity like the *T. brucei* procyclics upon Hesperadin mediated inhibition. These results highlight the diversity in protein homologs of even phylogenetically close organisms. Further investigations into the diverse functions of *Leishmania AIRK* and as a potential chemotherapeutic target are warranted. Notably, we provide a platform for further analysis of other potential drug targets identified in this study. The journey of discovery is clearly far from over for Aurora kinases.

2. Materials and methods

2.1. Database and sequence analysis

TritrypDB version 3.2 (http://tritrypdb.org/tritrypdb/) and TDRtargets (http://tdrtargets.org/) was used to select novel druggable targets in kinetoplastid parasites. The nucleotide and amino acid sequences of selected proteins (from kinetoplastids such as *L. major, L. infantum, L. donovani, L. braziliensis, T. brucei* and *T. cruzi)* were retrieved from the GeneDB gene database and those from *S. cerevisiae* and *S. pombe* , *C. elegans, D. melanogaster* and mammals from the NCBI nucleotide and protein database. BLAST searches were performed via the NCBI (http://blast.ncbi.nlm.nih.gov/Blast.cgi) and genedB databases (http://www.genedb.org). The nucleotide and protein sequences from different kinetoplastids were searched using the *L. donovani* homolog as the query sequence. GenBank accession numbers of the Ld*AIRK* nucleotide and protein sequences were (XM_003862106) and (XP_003862154), respectively. The accession identifiers of all selected proteins are mentioned in (Supplementary Table S1). The shortlisted candidate proteins from the above survey were subjected to further BLAST analysis using the human homologs as the query.

2.2. Amino Acid Sequence Alignments and Molecular Phylogeny Analyses

Multiple sequence alignments of full-length Ld*AIRK* sequence was computed using ClustalW version 2.1 and analyzed using Jalview version 2.0 [26]. Phylogenetic analysis of selected kinases was performed with the help of MEGA software version 6.0 [27] by using the neighbor-joining method based on the bottom-up clustering algorithm. Evolutionary distances were computed using the Poisson correction method and bootstrap analysis with 1000 replicates were carried out to obtain confidence level with the branches.

2.3. Cloning, Expression, and Purification of C-terminal His-tagged LdAIRK

Total mRNA was isolated from the *L. donovani* AG83 strain and converted into cDNA. The Ld*AIRK* ORFs subsequently amplified using Taq DNA polymerase as part of a FastStart High Fidelity PCR System (Roche). Primer sequences used were: Forward primer: 5'ATTCCATATG ATGACGACGGAGGTCGG-3'; and Reverse primer: 5'GCGGGATCCCTAATGATGATGA TGATGA TGGCTGCGCGGTCGCTTTCCCG-3', designed to include the NdeI and BamH1 restriction sites respectively, based on the gene corresponding to Acc.No. XM_003862106.1 as template. The 340-bp DNA product was subsequently ligated into expression vector pET11b (Novagen). *E. coli* BL21 competent cells (Rosetta strain) were transformed, and expression was induced by the addition of 1mM isopropyl 1-thio-β-galactopyranoside at 30 °C overnight. Cells were then lysed by sonication and addition of lysozyme (1 mg/ml). Recombinant proteins were purified using Ni^{2+}-NTA columns (Qiagen), eluted with 500 mM imidazole, and stored in a Tris-HCl buffer, (pH 8.0) diluted with glycerol 1:1 (v/v) at -80°C. Protein concentrations were determined by Lowry method [28] and purity checked by SDS-PAGE, followed by staining with silver nitrate [29].

2.4. In-gel tryptic digestion, Mass Spectrometry and Database Searching

The band corresponding to Ld*AIRK* was excised from the SDS-PAGE gel after colloidal Coomassie staining and sliced into small gel pieces and processed as per the kit instructions. Subsequently, both mass spectrometry (MS) and MS/MS spectra were obtained by MALDI-TOF/TOF mass spectrometer (Applied Biosystems 4800 Proteomics Analyzer). All spectra were collected in the reflector mode. Database searching for confirmation of protein identity was carried out using GPS Explorer (Applied Biosystems) software with MASCOT (Matrix Science) search engine [30].

2.5. Antibody generation

Female BALB/c mice (6 weeks old) were immunized by subcutaneous immunization of 25 µg of recombinant Ld*AIRK*. Protein was applied with Complete Freund's adjuvant (1:1, v/v) in the first immunization, followed by two booster injections at days 21 and 42, using Incomplete Freund's adjuvants (1:1, v/v). Ten days after the last immunization serum was collected for testing antibody titer and reactivity [31].

2.6. Circular Dichroism Experiments

Far-UV (260nm-200nm) CD-spectra were obtained using a Jasco-815 spectropolarimeter (Applied Photophysics) calibrated with ammonium (+)-10 camphorsulfonate. All measurements were collected in quartz cells of 0.1 cm path length with a scan-speed of 50 nm/min, bandwidth 1nm and temperature of 20°C in 0.02 M PBS pH 7.0 except for the pH optima studies (Supplementary Table S2). The effect of ATP and Hesperadin was observed in the concentration range 0–200 µM. The spectral shifts in apo or complex with ATP or Hesperadin or upon pH variations were performed using standard protocol [32]. The K2D3 software (http:// www.ogic.ca/projects/k2d3/) was used to analyse the spectra [33]and plotted after smoothing using the Savitzky Golay algorithm (OriginPro8).

2.7. Homology modeling

The templates used for homology modeling were found by searching for structures with maximum identity, using blastp which uses the amino acid sequence as input and generates an alignment profile. Four structures from PDB were generated as potential templates - all mammalian AURKA or B structures (PDB IDs- 4AF3_A, 3D14_A, 3DAJ_A, 2WTW_A). The human structure- 4AF3_A was used as the template for homology modeling which was carried out using Modeller 9.12 [34] under default parameters with the pair-wise sequence alignment file of the target (Ld*AIRK*) and template as inputs. Five models ranked on the basis of their minimum internal energy were produced as modeller outputs. The model with minimum internal energy and root mean square deviation from the template was used for further validation. The model was validated using Procheck and visualized using UCSF Chimera [35].

2.8. Preparation of ligands, protein, prediction of active site and docking

Schrodinger 2015 molecular modeling software was used to explore the ligand-enzyme interaction. Glide® integrated with Maestro 10.1 v101012 (Schrödinger LLC, 2015) was used for docking. Ligand molecules were built using Maestro 10.1 v101012 build panel. Ligands were prepared by Ligprep 3.3 v33012 application using OPLS–2005 force field for the energy minimization of the ligand. Homology modelled structure of Ld*AIRK* was prepared by the protein preparation wizard bundled with the Maestro Schrödinger package and includes the addition of hydrogens, assigning partial charges, assigning protonation states and energy optimization with the OPLS–2005 force field. A maximum root mean square deviation (RMSD) of 0.30 Å from the original structure was allowed for the constrained minimization steps. The energy minimized protein was used for the prediction of the possible active site. The primary binding site on the enzyme was unknown since the modelled enzyme was devoid of associated co–crystallized ligand. Therefore, the possible potential binding cavities within the receptor was predicted by using the Sitemap® 3.4 v34012 module in Maestro Schrödinger® 10.1 v101012. The sitemap centroid with the highest site score of 1.071 was utilised for the generation of grid (Supplementary Table 1 and Supplementary Figure S1and S2). Receptor grid was generated within the contour of the predicted active site [36]. The energy minimized ligands were docked into prepared grids with XYZ coordinates (18.24, -24.28 and -0.19) using Glide XP (Extra precision) mode of Glide 6.6 v66012 [37].

2.9. Parasite and Cell Culture

L. donovani amastigotes of AG83 strain (MHOM/IN/83/AG83) were maintained by serial passage in Syrian golden hamsters as described earlier [38]. Promastigote forms of the parasite were cultured at an average density of 2×106 cells/ml in medium M199 (Himedia) supplemented with 10% fetal calf serum and antibiotics at 26^{o}C [39].

2.10. Creation of Null Mutant

In order to genetically remove the XM_003862106.1 (Ld*AIRK*) open reading frame (ORF) sequences surrounding the Ld*AIRK* ORF were amplified using the following primers containing SfiI sites (underlined) compatible with a previously described method to rapidly generate knock-out constructs [40-41]: 5'TS-forward (A) gaGGCCACCTAGGCCGTGCGCGCGTATGTGC TTGTG, 5'TS-reverse (B) gaGGCCACGCAGGCCTATCTCTACGGTTTGTGACGT, 3'TS-forward (C) gaGGCCTCTGTGGCCCGAGACATGCCACAGGGAGGG, 3'TS-reverse (D) gaGGCCTGACT GGCCTCGACCTTACCGACTAC CAGCA. Linear targeting constructs were excised by restriction digestion using Pac1 and gel purified before transfection using a GenePulser XCell (Bio-Rad) system as described previously [41]. Transfected parasites were allowed to recover for 48 hours before addition of 20 μg/ml hygromycin for selection.

2.11. Confocal Microscopy

Five days infected macrophages on poly-lysine coated slides (Genetix) or log phase promastigotes, washed and airdried on 10mm coverslips were methanol fixed for 20 min followed by blocking with 5% goat serum in PBS for 30 min prior to probing with antibodies. Mouse anti-Ld*AIRK* antibody (Lab raised) was used to probe Ld*AIRK* overnight at 4°C, washed thrice in PBS 0.01%Triton-X and incubated for 1 h at room temperature with goat anti-mouse secondary antibody conjugated to FITC (Genei, Bangalore, India). All washes were performed at room temperature. After immunostaining, the coverslips were mounted on a glass slide using mounting media with DAPI (Molecular Probes). Images were captured by Andor spinning-disk live-cell confocal/ TIRF microscope (Andor Technology, Belfast, United Kingdom).

2.12. Flow cytometry-based sorting

Exponentially growing *L. donovani* promastigotes were gently washed and resuspended (at a concentration of $5x10^6$ cells/ml) in 1xPBS supplemented with 5% FCS and 5 µg/ml Hoechst 33342 (Molecular Probes). After incubation for 1 h at 26°C in the dark, the stained cells were sorted on the FACS Aria sorter (BD) based on the DNA content and collected in three tubes placed on ice, pelleted and stored at -80°C until further processing. [42-43].

2.13. mRNA Quantification

Total RNA was extracted using TRIzol reagent (Invitrogen), purified on RNeasy Mini Kit column (Qiagen) and quantified using a NanoDrop ND-1000 spectrophotometer (Thermo Fisher Scientific). DNase digestion was carried out during RNA extraction using RNase-free DNase Set (Qiagen). RT-PCR was performed for the LdGAPDH (housekeeping) and Ld*AIRK* (target) genes in a LightCycler 480 (Roche) using 100 ng of RNA. Relative quantification was performed using the Pfaffl method [44].

2.14. Western Blot Analysis

L. donovani promastigotes were lysed in lysis buffer containing 20 mM Tris-HCl, pH 8.0, 0.14 M NaCl, 10% glycerol, 1% NP40 and 1 mM PMSF (protease inhibitor), and incubated on ice for 30 min and centrifuged at 15K rpm for 10 min at 4°C. The supernatant was collected and protein concentration estimated by Lowry assay. About 60 µg of protein/lane was resolved on a 12% SDS-PAGE and transferred to nitrocellulose membrane (Millipore). The membranes were blocked with 2% BSA overnight at 4°C, and incubated with either (1:5000 dilution) rabbit-anti-Actin antibody (Santa Cruz Biotechnology) or (1:10000 dilution) mouse-anti-Ld*AIRK* antibody. After washing thrice with 0.05% Tween in 20 mM Tris-buffered saline pH 7.5 (washing buffer), the membranes were incubated with goat-anti-rabbit IgG-HRP antibody (Santa Cruz Biotechnology) or goat-anti-mouse IgG-HRP antibody (Santa Cruz Biotechnology). After further washes, binding was detected by incubating with ECL substrate (Pierce) and documented using Chemidoc (Bio-Rad). The densiometric analysis was performed using ImageJ (NIH, USA).

2.15. Enzyme Assays and Determination of IC50

Kinase activity was measured at 37 °C by the addition of 50 ng of Ld*AIRK* to 50µl of 20 mM HEPES, pH 7.4, 150 mM KCl, 5 mM MgCl2, 5 mM NaF, 1 mM DTT and 5 µg of myelin basic protein (MBP) (Invitrogen) or recombinant histone H3 from *L. donovani*, LdH3 (obtained from Dr. A. Dube, CDRI, Lucknow) as substrate [45]. Upon addition of 8 µM ATP (4 µCi of [γ-^{32}P]-ATP), the reaction was incubated for 10 min at room temperature, other than the time course experiment. Reactions were stopped with 5x Laemmli buffer, and proteins separated on a 10% SDS-PAGE gel. Post-run, gels were stained with Coomassie blue, dried on a Gel Slab Dryer (Bio-Rad), and analyzed using a PhosphorImager (Molecular Dynamics). Quantification of phosphorylation was performed using ImageJ (NIH, USA). For IC50 determination, the inhibitory effect of Hesperadin, Barasertib or GSK-1070916 (SelleckChem) were determined by the pre-incubation of Ld*AIRK* with the respective drug (within the concentration range of 0-100ug/ml) for 30 min before adding the substrate, ATP. Activity (% control) of a certain sample was calculated using the following formula:

Activity (as % of plus enzyme sample) = Band intensity (experimental sample – no enzyme control) /

Band intensity (plus enzyme control– no enzyme control) x 100

The non-radioactive assay was performed for the time course experiments to determine the Michaelis- Menten constants. These were carried out in a 96-well format using the Universal Kinase Assay Kit (R&D). All reactions were performed as per the kit instructions [46]. The formation of malachite green/molybdate complex was recorded (Abs 600 nm) over 10 min at 1 min intervals at 37 °C, in which the concentration of ATP was varied between 0 and 200 µM. Reported kinetic parameters derive from nonlinear regression fits of the data using GraphPad Prism 5 (GraphPad Software).

2.16. Isolation and Infection of Mouse Peritoneal Macrophages

The peritoneal cavities of mice were flushed with 5 ml of ice-cold RPMI 1640 medium (Himedia) supplemented with 50 µM β-mercaptoethanol and 10% FCS (pH 7.4). After centrifugation and washing, 10^6 cells were plated on sterile glass coverslips in 24-well tissue culture plates and incubated overnight at 37°C with 5% CO_2. Nonadherent cells were removed by washing three times with prewarmed PBS. Stationary phase promastigotes were used to infect these cells at a ratio of 10:1, for 3 h, washed and the infection allowed to proceed for 5 days.

2.17. Antiproliferative Assays

Growth inhibition of *L. donovani* amastigotes was monitored as described below. Mouse peritoneal macrophages were plated and infected as explained above, incubated overnight in a 5 % (v/v) CO_2 incubator maintained at37°C, washed twice with RPMI to remove non-internalised parasites and incubated with fresh media containing different concentrations of the drugs. Following incubation for another 72 hours, the cells were washed and fixed in methanol

followed by Giemsa staining. The amastigotes in differentially treated macrophages were counted and the IC50 values determined. For study in promastigotes, logarithmically (5-6 x 10^6 cells/ml) growing cells were diluted to 2 x 10^6 cells/ml and incubated with various concentrations of each drug at 26°C for 24/28/72 hours before the addition of the Alamar Blue (0.01%) (Invitrogen). After another 16 h of incubation, the absorbance of the reduced resazurin was measured (570 nm and 600 nm) [47]. Cells grown in the presence of 0.2% DMSO were treated as control (100%), and percent viability was plotted as a function of concentration. All assays were performed in 96-well cell-culture plates, and IC50 values estimated using GraphPad Prism. Treatment with amphotericin B (1mg/ml) for 72h was taken as the positive control (100% killing or positive control). % Viability was calculated using the following formula with the value of Blank wells subtracted from all readings:

$$\%\ \text{Viability}_{\text{Promastigote}} = \left[\Delta OD_{(570\text{-}600)\text{Treated}} / \Delta OD_{(570\text{-}600)\text{Untreated}}\right] X100$$

$$\%\ \text{Viability}_{\text{Amastigote}} = \left[\text{No. of parasite per 100 macrophages}_{\text{Treated}} / \text{ No. of parasite per 100 macrophages}_{\text{Untreated}}\right] X100$$

2.18. Accession number

XM_003862106.1

2.19. Statistical Analysis

Results are presented as means ± S.E.M. Statistical differences between two groups were determined with Student's t-test, and differences between multiple groups were determined using One-way ANOVA followed by Tukey's multiple-comparison test. P values of 0.05 were considered significant. All analyses were performed using GraphPad Prism software.

3. Results

3.1. Identification, sequence analysis, cloning and purification of LdAIRK.

Our understanding of key pathways in human visceral leishmaniasis (VL) remains limited. Based on the methods described under 'Experimental Procedures' we identified various components of cell signaling, gene regulation, cell division, protein export and transport that play central roles in some core parasite processes. The sequences of sixty such proteins were retrieved from the geneDB database for the BPK *L. donovani* strain followed by BLAST analysis of the genome databases of *L. major, L. braziliensis, L. infantum, T. brucei* and *T. cruzi* which yielded 12 members as top scorers based on their sequence conservation (Supplementary Table S1). To further investigate their presence and distance from the host proteome, these were used as the query and subjected to BLAST analysis, against the human protein database from NCBI. This allowed the identification of four candidates least homologous to their human counterparts

(Table 1). Amongst these, a putative protein kinase (Acc. No- LdBPK_ 280 550.1) was selected for further characterization. Upon sequence analysis it was found to be an Aurora-like kinase which has been described in various organisms, playing pivotal roles in the control of cell division. *L. donovani* encodes a 3 membered family of Aurora kinases – (Acc. No- >LdBPK_ 280550.1.1..pep, >LdBPK_291420.1.1..pep, >LdBPK_262460.1.1..pep) , with a single copy of each. Together with sequences of homologs from other organisms, the sequence corresponding to Acc. No-LdBPK_280550.1 was subjected to multiple sequence alignment (Figure 1A). Inter-species comparison revealed sequence identity between 79-100 % which reduced to only 44% when compared to human Aurora kinases. Most of the differences lied in the N and C-terminal domains, *e.g.*, the missing KEN box region in the *Leishmania* homolog. Of interest, some blocks of sequences were highly conserved in all the sequences compared (Figure 1B). These were annotated as per the nomenclature used for human Aurora kinase domains [48], namely the (i) Nucleotide binding domain (GGNYGDVY) and (LEPC); (ii) T-loop domain (DFGWSVHDP LNRRKTSCGTP EYFPPE) and the (iii) D-box domain (LLIREGSK RLALHRVLSHPF). Using the structure of human Aurora kinase A (PDB ID-4AF3_A) as the template (top-most hit in a BLAST search), a homology model of Ld*AIRK* was created (Supplementary Figure S1A). The residues in the conserved domains of the protein are highlighted with an identical colour scheme as used in the schematic diagram to aid comparison. Furthermore, a phylogenetic analysis with all Aurora kinases characterized till date as well as putative ones was generated (Supplementary Figure S1B). This phylogram revealed the *T.brucei* homolog (Acc.no.XP_828896.1) to be the closest characterized homolog [13]. Located on chromosome 28, Ldairk was found most similar to the *D. melanogaster* Aurora kinase (Aurora-A), with 61% identity over 794 bp. On the protein level, it reduced to 46% over 261 amino-acids of *D. melanogaster* Aurora-A, 39% identical over 264 amino-acids to Ipl1p of *S. cerevisiae* (Ipl1) and 42% identical over 275 amino-acids of *H. sapiens* (Aurora-B) among the higher eukaryotes. This similarity was significantly improved upon comparison with *T. brucei*, being 80% identical over 299 residues and 98% over 300 residues in the case of *L. major*. Surprisingly, the *P. falciparum* homologs exhibited the least homology.

Notably, the closest human homolog- Aurora B was also quite distantly located. Hence, as a part of the ongoing HOPE project, the gene corresponding to Acc.no. LdBPK_280550.1 was cloned with a C-terminal His-tag into the bacterial expression vector pET11b (Supplementary Figure S1C). It was subsequently purified using a Ni_2-NTA column (Qiagen) at a concentration of approximately 5 mg/ml to be used for biochemical, biophysical and functional analyses. To confirm the identity of the cloned protein we carried out MALDI-TOF MS and MS/MS analysis of the band corresponding to purified Ld*AIRK*, silver stained to assess its purity on an analytical SDS-PAGE gel (Supplementary Figure S1D, S1E and S1F). It was subjected to in-gel trypsin digestion, and the resulting peptides were searched against the NCBI protein database. The MASCOT search algorithm indicated the best match having a score of 427 and sequence coverage of 56% to a putative protein kinase from *L. infantum* and subsequently with Lmairk, a member of the Aurora/Ipl1p family of protein kinases from *L. major*. It predicted a molecular

weight of 34.9 kDa and a PI of 8.21. Mouse polyclonal antibodies were raised against rLd*AIRK* purified from *E. coli* to confirm the size and localization of the endogenous protein by western blotting and immunofluorescence assays, respectively. The total lysate of *Leishmania* parasite was analyzed by SDS- PAGE followed by immunoblotting with antibodies specific for Ld*AIRK* (Supplementary Figure S1G). The calculated molecular mass of 35.4 kDa was in concert with the predicted molecular mass of 34.9 kDa with the slight difference arising due to the presence of a poly-histidine tag. This also confirmed the purity and specificity of the antibodies.

3.2. Cell-cycle regulated expression and localization of LdAIRK

Aurora kinases in complex with other proteins are known mediators of chromosome segregation and perform their functions at restricted subcellular locales. We investigated the spatio-temporal subcellular localization of endogenous Ld*AIRK* using antibodies raised in mice. As a first step, we confirmed that both the promastigote and physiologically significant amastigote stages of the parasite express Ld*AIRK*. Mice peritoneal macrophages infected and stained after 5 days when parasite infection reached its peak before macrophage disintegration and amastigote release, demonstrated rings of Ld*AIRK* expression surrounding the parasite nucleus in all the amastigotes (Figure 2A). However, some non-specific interaction, probably with the macrophage nuclear Aurora kinases was also observed. Further investigations were carried out in the promastigote stage of the parasite, to assess the dynamics of their localization and predicted role based on its position, as the cell-cycle progresses. Actively growing parasite cultures were co-stained for Ld*AIRK* and the nuclear and kinetoplast DNA, which are good markers of the cell division cycle [49]. Representative cells from each phase were observed and characterized. As shown in (Figure 2B), Ld*AIRK* undergoes dramatic redistribution during cell division. During the G0/G1 phase, the endogenous Ld*AIRK* shows limited expression and are localized to the cytoplasm in a nucleus excluded pattern, also predicted by the TMHMM (version2.0) server due to the absence of any transmembrane domains (Figure 2*B, upper panel*). As the cell enters S phase, a dramatic increase in Ld*AIRK* expression is noted. These are concentrated at the nuclear periphery, mostly at the centrosomal region (Figure 2*B, middle panel*). Ld*AIRK* remains at the centrosomes as the cell enters G2/M. Moreover, their expression is now considerably heightened and more focussed at the two poles (Figure 2*B, bottom panel*). To validate the immunofluorescence experiments, we performed RT-PCR and western blot analysis of pure cell population from each cyclical phase. Logarithmically growing parasites were stained with the vital DNA dye Hoechst and sorted based on their DNA content into G1, S and G2M phase. The dot–plots of the sorting experiments are provided in the (Supplementary Figure S2). The purity of the sorted cells was confirmed by post-sort FACS analysis as well as fluorescence analysis (Supplementary Figure S2C and S2D). The G1 sorted cells showed a single distinct nucleus and kinetoplast DNA. At S phase, the increased fluorescence intensity of the nuclear matter and the central bulge was noted. Lastly, the G2/M phase population clearly depicted dividing cells with double the nuclear and kinetoplast DNA content.

Using these phase-separated cells, total RNA was isolated and analyzed by RT-PCR and the differences were clearly reflected by the Ct values. With GAPDH as the house keeping control, Ld*AIRK* expression depicted an increase by 1.7-folds in the S phase and 2-folds in the G2M phases of the cell-cycle compared to the G1 phase (Figure 3A). The details of this experiment are summarized in (Supplementary Table S3). To analyse regulation of Ld*AIRK* expression at the translational level, total parasite lysate of the sorted cells was subjected to SDS-PAGE followed by western blotting. Using actin expression as the loading control, the protein levels depicted a pattern similar to that seen by immunofluorescence and RT-PCR studies. The S phase cells showed expression that was almost 1.64-fold greater as compared to G1 stage cells which increased by 1.86-folds at the G2/M phase (Figure 3B). Taken together, Ld*AIRK* was found to exhibit a cytosolic localization with re-localization around the nuclear periphery and poles, from S phase until cytokinesis.

3.3. LdAIRK has ATPase activity and is sensitive to inhibition by Hesperadin but not Barasertib or GSK-1070916.

In order to evaluate the proper folding of recombinantly expressed Ld*AIRK*, CD experiments were performed. Alpha-helical content of 27.78%; beta sheets- 24.38% and random coils- 47.84% was calculated (Supplementary Figure S4A), in agreement with those predicted by the PHD server (Supplementary Table S4). Additionally, because *L. donovani* experiences a digenetic life cycle and hence different pH environments, we evaluated the stability of the enzyme under different pH conditions (Supplementary Figure S4B). The studies showed that rLd*AIRK* exhibits maximum stability in the pH 7-8 range, with a rapid loss in spectral intensity even upon single unit pH shifts on either side. In order to functionally characterize the enzyme, its phosphotransferase activity and substrate specificity were studied in an *in vitro* kinase assay. In addition to trans-phosphorylation of MBP (generic substrate) and LdH3 (physiological substrate), auto-phosphorylation of the kinase and a truncated form was also observed (Figure 4A). Furthermore, by measuring initial reaction velocities at saturating LdH3 concentrations, we found that Ld*AIRK* exhibited typical hyperbolic Michaelis-Menten saturation kinetics (Figure 4B). We determined a Km of 6.12 uM, Vmax of 82.9 pmoles.min^{-1}mg^{-1} and Kcat of 2.905 s^{-1} towards ATP. However, upon addition of different dNTPs (dATP/GTP/TTP/CTP) as competing phosphate group donors, only ATP seemed to inhibit substrate phosphorylation (Figure 4C). Hence, ATP alone can act as the phosphate donor for these kinases.

Subsequently, three existing and structurally distinct mammalian Aurora kinase inhibitors were probed for their ability to dock into the active site of Ld*AIRK* (Supplementary Figure S4C and Supplementary Table S5) and further explore the nature of the enzyme. Although all three are reversible ATP-competitive inhibitors (Figure 5A, *upper panel*), they differ considerably in both affinity and target preference. Hesperadin is mainly an Aurora B inhibitor having an IC50 of 250 nM *in vitro*. However, it reduces the activity of some other kinases too. On the other hand, Barasertib is highly selective with an IC50 of 0.37 nM for Aurora B but inhibits Aurora A too, although with lesser affinity. The third inhibitor GSK-1070916 inhibits both Aurora B and

C with IC50 of 3.5 nM and 6.5 nM, respectively (Selleck Chemicals). The idea was to characterize the kinase more finely based on its inhibition behavior and get leads for the development of more refined structures built on the success of some existing inhibitors. The G-scores obtained were -7.79 for Hesperadin, -7.28 for Barasertib and -7.61 for GSK-1070916 respectively (Table 2). LigPlot analysis showed that the residues Asn 41, Phe 173, Gly 174, Phe 173, Asn 121 and Lys 60 take part in the H-bond formation with the test ligands. Hesperadin can form two H-bond's with Asn 41 and Phe 173 as focused in yellow colour in (Figure 5A, *lower panel).* Whereas, Berasertib can form 3 H-bond's with Phe 173, Asn 121 and Lys 60; GSK-1070916 can form only 1 H-Bond with Gly 174. Although the G-scores for Hesperadin and GSK-1070916 were only slightly different (0.19), the bond strength (to which the number and length of H-bonds both contribute) predicted Hesperadin to have the best binding affinity with Ld*AIRK* (Table 2).

Hence, we examined the extent of drug-mediated inhibition of Ld*AIRK* by monitoring the transfer of γP^{32} from γP^{32}-ATP to LdH3 substrate by incubating equal concentrations of Ld*AIRK* with increasing concentrations (10-100 ug/ml) of the respective drug. The residual kinase activity was plotted against $\log_{10}$ (Drug concentration). Ld*AIRK* was found to be insensitive to Barasertib or GSK-1070916 mediated inhibition even at 200μM concentration (Fig. 5C, *middle* and *last panel*). However, upon incubation with Hesperadin, a hyperbolic inhibition curve indicated competitive binding with an IC50 of 44.20±1.58 nM (Figure 5B). Despite Ld*AIRK* being modeled on the crystal structure of human Aurora B as the template, the inhibitors with lower IC50 for human Aurora kinases – Barasertib and GSK-1070916 were ineffective against Ld*AIRK*, whereas, Hesperadin with a 10-fold higher IC50 showed considerably greater inhibition of Ld*AIRK*. This interaction was further seen in the spectral shifts of Ld*AIRK* in the presence or absence of these ligands as observed by CD spectroscopy. Hesperadin being an ATP-competitive inhibitor, equal concentrations of purified Ld*AIRK* were incubated with varying concentrations of ATP or Hesperadin and the spectra recorded in the far U.V. range. The ATP-bound and free forms exhibited marked differences in the CD spectra (Supplementary Figure S4D). Hence, Hesperadin binding should also produce such a shift as it binds the same domain of the protein as ATP. However, although evident, the shifts were not identical in both cases (Supplementary Figure S4E). Hence, their mode of binding and, therefore, the conformations adopted are probably different.

3.4. LdAIRK activity is essential for both promastigote and amastigote forms of L. donovani.

The results from *in vitro* experiments demonstrated the effectiveness of Hesperadin over Barasersib and GSK-1070916 against Ld*AIRK* activity. To determine the physiological relevance of this inhibition, the amastigote and promastigote stages of the parasites were incubated with various concentrations of the drugs under study and the effects evaluated. Infected peritoneal macrophages having approximately 4-6 parasites/macrophage were treated with varied drug concentrations for 72 hours before assessing the parasite load. A 50% reduction in parasite load was seen at ~36.4±2.12 nM (Figure 6A). Moreover, we observed complete parasite clearance

above 480 nM although accompanied by macrophage disintegration. Also, the CC50 (50% cytotoxic concentration towards host cells) was found to be in the micromolar range, almost 30-folds higher than the IC50 observed for amastigotes, thus ruling out any effect of macrophage cytotoxicity on the parasite load (Supplementary Figure S6,7). For the studies on promastigotes, each of the inhibitors was added to logarithmically growing cultures and the cell numbers quantified over time. Also, the reducing environment, characteristic of healthy cells, was evaluated by Alamar blue reduction assay (Figure 6B). Upon inhibition with Hesperadin, parasite growth was severely compromised. At 24 hours, an IC50 of 692.3± 29.3 nM was observed, which reduced to an IC50 of 632±42.6 nM after 48 hours of treatment. By this time, almost all the cells appeared swollen having more than twice the size compared to untreated cells. At 72 hours, most of the cells had attained a ginger-like shape with many roundish protrusions with the IC50 decreased 6-fold. Moreover, most cells demonstrated a rudimentary or total flagellar loss. Eventually, all parasites died at this concentration, and necrotic debris was observed. These morphological changes occurring over time have been presented in Figure 8A. In contrast, parasites growing in the presence of Barasersib or GSK-1070916, grew robustly even after 72 hours of drug treatment without any apparent morphological change.

To determine whether the growth defect in the presence of Hesperadin occurred as a result of interrupted cell division, and in case these kinases are involved in cytokinesis like their homologs in other organisms [50-52] cell-cycle progression was monitored by flow cytometry at 24, 48 and 72 hours post drug treatment (Figure 7A). As hypothesized, the growth defects observed were accompanied by an increase in total DNA content. Cells with 2C DNA content, which represents the G0/G1 population, rapidly decreased from 61.12% at 0 hours to only 10% at 72 hours post treatment. Cells with 4C DNA content (representative of the G2M phase) gradually rose and formed >48.6% of the population after 24h of incubation with drug, demonstrating a G2/M block. Simultaneously, cells with >4C DNA content, which includes both the 6C and 8C populations, increased from 3% at 0 hours to 38.5% after 72hours. In addition, the sub-G_0 fraction increased from 1.7% at 0 hours to 17.2% after 72 hours, indicating nuclear fragmentation, probably due to cell death. The time-dependent changes in cell populations of different nuclear content are depicted in (Figure 7B). Interestingly, the unusual changes in ploidy and apoptotic DNA content were not observed until 48 hours of incubation.

Fluorescence microscopy of fixed and DAPI stained cells provided a qualitative analysis of these observations. An abundance of nuclear matter, both genomic and kinetoplast, was clearly visible (Figure 8A). A gradual increase in 2N2K and 2N1K cells with a collateral decrease in 1N1K and 1N2K cells was observed from 24 hours through 72 hours of treatment. Following incubation with Hesperadin, 2N2K cells, which formed only 4% of the population in untreated cells, soared to over 33% of the population at 48 hours. At 72 hours, this rose to 57.8% of the total population. Further study revealed that nearly 81% of these 2N2K cells had not yet completed mitosis, with only around 18% showing 2 distinct nuclei. Moreover, a subset of cells

with undivided nuclear matter but the intensity of >4N the DNA content was observed in giant spheroid cells devoid of any flagella. These changes are graphically depicted in (Figure 8B).

These data strongly suggest that Ld*AIRK* may play a crucial role in mitosis and cytokinesis and perturbations in their regulation shift the balance towards increased ploidy and ultimately growth arrest and death.

4. Discussion

Since their discovery in the 20th century [53-54], Aurora kinases have emerged as a critical mediator of the cell division cycle in *H. sapiens, Xenopus, Drosophila,* and *C. elegans.* In recent years, their regulatory roles have been established in lower eukaryotes like yeast, parasitic protozoa like *Plasmodium* and *Trypanosomes* as well as plants [15, 52,55]. Most organisms have more than one type of these kinases. Together, they play diverse roles in mitosis and meiosis, including centrosome maturation and separation, spindle assembly, chromosome biorientation, condensation, cohesion and segregation followed by cytokinesis [53, 56-61]. Aurora kinases mediate their effects by phosphorylating their targets, histone H3, cytoplasmic polyadenylation element binding protein CPEB, tumor suppressor protein p53, PP1 protein phosphatase 1 isoforms, INCENP, CENP-A, mitotic centromere associated kinesin MCAK and vimentin (http://kinasource.co.uk/Database/substrates.html). The pivotal role played by them as evident by the substrate diversity, has been exploited by implicating them as therapeutic targets in various infectious as well as non-infectious diseases [19].

In this study, an Aurora kinase homolog from *L. donovani* was identified and named Ld*AIRK* based on its 98% amino acid sequence identity with Lm*AIRK* from *L. major* [14]. Here, we have for the first time carried out a systematic bioinformatic, biochemical, biophysical and functional characterization of a full-length rLd*AIRK* as well as examined its importance in intracellular amastigotes and an *in vitro* growing culture of *L. donovani* strain AG83 promastigotes. Their primary structure demonstrates significant homology to other characterized Aurora kinases with significant sequence conservation in the three domains. Moreover, among the three isoforms identified in the *L. donovani* genome, only Ld*AIRK* was found to have all the identifying domains characteristic of Aurora kinases with 80% identity to the closest characterized homolog, TbAUK1 from *T. brucei*. However, the sequences corresponding to >LdBPK_291420.1.1..pep and >LdBPK_262460.1.1..pep showed only 53% and 29% identity to the putative homologs from *T. brucei.* Interestingly, the *P. falciparum* homologs which proved essential in gene knock-out experiments were significantly different from their *L. donovani* counterparts. Following cloning and purification, MALDI-TOF MS/MS analysis confirmed the identity of the protein which was then used to raise polyclonal antibodies in mice and checked for their specificity by immunoblots of parasite lysate.

Subsequently, the spatio-temporal expression pattern of native Ld*AIRK* was studied by immunofluorescence microscopy. The staining of infected macrophages revealed their cytosolic

expression in the amastigotes, localized outside the DAPI stained nucleus and kinetoplast. Further studies were carried out in the promastigote stages, wherein the cell-cycle stages were designated by the position, qualitative and quantitative analysis of their nuclei and kinetoplast and also by the overall cellular morphology. The expression of Ld*AIRK* was seen to increase significantly as the cells progressed from G1 to S phase and was retained until mitosis. The diffuse distribution of Ld*AIRK* in the cytoplasm of G1 phase cells was vastly over-expressed and much concentrated at the nuclear periphery near the centrosomal poles in the S phase, in line with their possible role as polar auroras involved in generating the central spindle for chromosomal attachment and subsequent segregation into daughter nuclei. Here, the nuclear DNA stained brighter compared to the G1 cells demonstrating the synthetic phase of the cell-cycle. Moreover, the kinetoplasts seemed elongated as seen just before their segregation. This was followed by a S to G2M transition phase wherein the majority of the cells depicted 1N2K phenotype. Herein, the endogenous protein was found concentrated predominantly at the poles of the single enlarged nucleus. In the G2M phase, the restriction in localization got even more prominent with Ld*AIRK* now more focussed at the two nuclear poles of the newly divided daughter cells. These distribution patterns are comparable to the localization patterns of an Aurora A kinase, which mediates spindle pole formation and chromosomal segregation [62]. Nevertheless, the active protein kinase pool could not be differentiated from the inactive forms in the absence of phosphospecific antibodies. Western blot and RT-PCR studies using pure populations of each cell-cycle phase (as sorted by FACS) moreover, supported these immunofluorescence observations. The immunoblots normalized to actin as house keeping control, reported a 1.64 and 1.86-fold increase in the S and G2M phases respectively as compared to the G1 phase cells. At the RNA level too, greater than 1.7 and 2.0-fold increase was observed (compared to G1 phase cells) in the S and G2M phases using GAPDH as housekeeping control. Thus, all these observations indicate a heightened expression of Ld*AIRK* at the DNA replication and division stages of the cell-cycle, pointing towards a possible role of Ld*AIRK* in these processes.

Next, the presence of secondary structural elements in rLd*AIRK* was confirmed by CD spectroscopy. Kinetic analysis under saturating LdH3 concentrations (the physiological substrate of both Aurora A and B), exhibited a catalytically active kinase. Under our experimental conditions, we observed a Km of 6.12 µM which was 2.5 and 4-times more than that observed for wild-type Aurora A and B, respectively. However, the catalytic efficiency, Kcat, at 2.905 s^{-1} was 10.8- and 1.5-times less than that observed for wild type Aurora A and B [63]. The lower catalytic efficiency observed in the *in vitro* kinase assays using pure Ld*AIRK* implies a lower rate of substrate cycling. Despite conservation in the overall T-loop sequence, from prokaryotes to eukaryotes, as demonstrated by the multiple sequence alignment, their abilities to bind and hydrolyze ATP differed. Possibly, parameters other than only the primary sequence (such as scaffolding proteins, post-translational modifications and sub-optimum experimental conditions) affect the enzymatic activity, not unlike the chaperone regulation of mammalian Aurora kinases [64].

For long, protein kinases have been proposed as potential drug targets in the treatment of diseases caused by trypanosomes and *Leishmania* [65]. As Ld*AIRK* function is dependent on its ATPase activity, we tested the effects of three human Aurora kinase inhibitors upon its activity, currently in various phases of clinical trial. We used Hesperadin (a first generation inhibitor), GSK- 1070916 (which has successfully completed phase I of the clinical trial) and Barasertib (which is in stage I of phase II clinical trial) to explore their ability to inhibit Ld*AIRK* activity. Firstly, we investigated the docking site of these compounds on the 3D crystallographic structure of Ld*AIRK* adopted by homology modeling. The active site (Sitemap_site1) was predicted by Sitemap® 3.4 v34012 on the basis of best site score value (1.071). In the docking procedure, the target protein was considered to be unbending, while the ligand was considered flexible. The ligands- Hesperadin, GSK-1070916 and Barasertib were docked into the appropriate binding pocket of Ld*AIRK* using Glide® integrated with Maestro 10.1 v101012 (Schrödinger LLC, 2015). The calculated binding energies increased in the order Hesperadin> GSK-1070916 >Barasertib. In addition to hydrophobic interactions, several H-bonds between the ligand and amino acid residues present in the active site of target enzyme also provide the driving force of binding with target pocket to inhibit its activity. According to the binding energy, docking pose and binding affinity in the hydrophobic pocket, Ld*AIRK* was found to be more sensitive to Hesperadin in comparison to other two test compounds (GSK-1070916 and Barasertib). Ld*AIRK* activity involves the residues: Phe 173, Asn 121 and Lys 60 and structural analysis reveals that amino- acid substitutions in the active site alters the catalytic activity of this enzyme. However, this remains to be verified experimentally. Most inhibitors target the conserved ATP binding site in the DFG (Phen-Asn-Lys) conformation or the allosteric site exposed through the classic DFG-flip. However, some inhibitors target an unusual nonDFG-out conformation called DFG-out (up) conformation (formed through ligand-induced conformational changes) thereby switching the nature of the active site from polar to hydrophobic. This conformation is formed when the DFG-loop is ushered to a location parallel to the αC-helix unlike the regular DFG-out wherein it swaps out of the active site. From the distance of the two atoms between ligand and target protein amino acids that form hydrogen bonds, we may conclude that Hesperadin could be designed as a stronger ligand towards Ld*AIRK*. It forms H-bonds of shorter length in contrast to the other two compounds. Additionally, from the shape of the binding pocket, Hesperadin may fit much better into it.

Following in-silico docking analysis, *in vitro* kinase assays using the physiological substrate LdH3 were performed. GSK-1070916 and Barasertib failed to have any effect on the phosphorylation of LdH3 by Ld*AIRK* within the range tested. On the other hand, Hesperadin was severely inhibitory towards LdH3 phosphorylation. However, only at an IC50 of 44.20 nM did it manage to deplete significantly the activity of Ld*AIRK*. Nevertheless, this was comparable to that achieved by the *T. brucei* homologue TbAUK1, which was 40 nM [45]. This may be explained by the highly similar sequence of the docking site of Hesperadin on these proteins (96% identity). It has been reported that for kinases sharing >60% identity over their catalytic domain, there is a high possibility of inhibition by the same molecules, thus suggesting a larger

probability of having common inhibitors selective for such kinases [66]. The three inhibitors tested differ in their mode and specificity of binding, Barasertib having an IC50 that is 650-folds greater followed by GSK-1070916 (between 38 to 70-folds greater) compared to Hesperadin [67-69]. Moreover, the differing affinity of Ld*AIRK* and mammalian Aurora B (over 5.6 –folds) towards Hesperadin yields preliminary confirmation that selective inhibition of these kinases is possible. Additionally, their inhibition by Hesperadin, suggests that Ld*AIRK*s are probably Aurora B homologues. The findings of the kinase assay justify the dry lab results of Hesperadin as a more potent inhibitor of Ld*AIRK*.

Taken together these results indicate that Ld*AIRK* is a promising target for therapeutic intervention. However, it was important to ascertain if Aurora kinase activity is essential for the parasites growth and propagation. Therefore, the effect of these inhibitors at various stages of the parasite's life cycle was measured using standard assays for parasite fitness. The *in vitro* growth effects of these inhibitors were validated by dose and time dependent studies on amastigotes as well as promastigotes. Just like the kinase inhibition studies, here too, GSK-1070916 and Barasertib failed to have any effect on the growth or morphology of the parasites. Since these inhibitors are specific for Aurora kinases, we may argue that either these inhibitors do not bind the *L. donovani* Aurora kinases, or if they do, then Ld*AIRK* does not have an essential role to play in the parasites growth. Since the kinase assays with purified Ld*AIRK* were also not affected by these inhibitors, the first hypothesis holds true. Furthermore, incubation of the promastigotes with Hesperadin led to drastically reduced survivability and altered morphology. This interaction was further validated by the shifts in CD spectra of Ld*AIRK* pre-incubated with Hesperadin compared to lone protein. Moreover, this interaction was positively proved in the kinase assays too, thus nullifying the second hypothesis. However, Hesperadin has multiple targets. Thus, the effects of their inhibition cannot be attributed solely to Ld*AIRK* inhibition. The importance of some of the other targets inhibited by Hesperadin, therefore cannot be ruled out. Furthermore, the intracellular amastigote forms of the parasite were also inhibited by incubation with Hesperadin at an IC50 of 36nM, demonstrating comparable inhibition profile to Hela calls in culture as well as *T. brucei* bloodstream forms [45]. Immunofluorescence and FACS analysis of DAPI and PI stained parasites (Hesperadin-treated) highlighted the pivotal role played by Ld*AIRK* (or other minor targets of Hesperadin) in the parasites life cycle. Upon treatment with increasing doses or incubation times with Hesperadin, a simultaneous increase in the parasites arrested at the G2M phase was observed with the G1 and S phase population greatly reduced. Moreover, after 48 hours of treatment, a new population started appearing at a greater fluorescence intensity, corresponding to >4C nucleic acid content. Probably, the cells entered a prolonged resting phase due to the stressful environment before resuming nuclear material synthesis. Hence, compared to untreated cells that undergo doubling in approximately 7-8 hours, it was delayed more than 5-fold in the treated cells. Interestingly, the nuclear DNA synthesis was not followed by their segregation in all the cells as observed microscopically. Although some cells showed a 2N2K phenotype with clearly segregated nuclei, most cells showed the same fluorescence intensity in FACS analysis but without any distinct segregation upon

immunofluorescence visualization. The difference in these phenotypes remains unexplained. Possibly, the cells showing clear nuclear segregation were in the G2M phase when the inhibitor was given which got arrested at that stage and were unable to proceed further, probably due to a role of Ld*AIRK* (or any other protein target) in cytokinesis. The other cells, with an undivided nuclear matter, however, suggest a blocked nuclear segregation but unaffected nuclear division upto 48 hours. The absence of any population beyond 8C, however, indicated that further nuclear synthesis was blocked after a second round of replication. Hence, Ld*AIRK* may play a role in chromosomal segregation as well. Notably the IC50 (Growth) value of 632 nM up to 48 hours, exhibited against *L. donovani* promastigotes were comparable with that for *T. brucei* cells (550nM). Further incubation up to 72 hours, reduced the IC50 by 6-folds, making it more effective. Our results suggest that *L. donovani* is sensitive to Hesperadin-mediated inhibition of Ld*AIRK* and is a close homologue of TbAUK1 [45]. Hence, a common inhibition programme may be successful for the eradication of these diseases.

Although there are many studies implicating inhibitors of Aurora kinases for the treatment of cancer, this is the first study demonstrating their importance towards the treatment of VL. Such an approach acquires significance, by not only saving enormous funds which are frugally provided for neglected tropical diseases, but also saving time by utilizing the existing knowledge base of chemotherapeutic targets and inhibitors. However, details regarding their structure-activity relationship with parasite proteins have only recently been reported [18] and much needs to be done towards the development of more specific inhibitors. As Hesperadin was shown to interfere with the development of *Leishmania, Trypanosoma* as well as *Plasmodium* [18], it may be possible to have a common therapy effective in treating malaria as well as trypanosomiasis and leishmaniasis in the near future. To summarize, we identified Ld*AIRK* an Aurora B homologue in *L. donovani* whose expression and distribution is cyclically regulated. Ld*AIRK* was found to possess a potentially essential role for both amastigote and promastigote survival demonstrating involvement in cell-cycle progression, specifically, chromosomal segregation and cytokinesis and appears to have a ligand specificity comparable with that of TbAUK1 and Aurora B. We found Hesperadin, an inhibitor with multiple targets though majorly Aurora B, to be detrimental to parasite survival. The discriminative nature in which Ld*AIRK* selectively binds to Hesperadin and not Barasertib or GSK-1070916, which are highly specific inhibitors of mammalian Aurora A/B and/or C, highlights significant differences in the kinase active site that could potentially be exploited in the development of new anti-parasite inhibitors. On a positive note, our study gave two insights. Firstly, it gave us a lead molecule in the form of Hesperadin, which can be further optimized hence saving much time and resources. However, its mechanistic aspects remain to be elucidated. Secondly, it was clear that the more specific inhibitors of mammalian kinases being ineffective against Ld*AIRK*, had no docking site. Hence, the active site in Ld*AIRK* is sufficiently different from their mammalian homologues to avoid the problem of un-intended ligand-protein interaction, thereby substantially increasing its druggability [70]. In addition, Ld*AIRK* was found to share properties of both A (in terms of localization), and B (with respect to their inhibition profile and manifestations) type Aurora kinases, demonstrating

similarity to Ark1 from *S. pombe*. In conclusion, our studies were based on the combined result of bioinformatic and wet lab analyses that led to the identification of more than one putative drug target, each of which warrant further biochemical and functional investigations. This study demonstrates that the *Leishmania* Aurora kinases are potentially elementary enzymes in insect stage *L. donovani*, providing chemical validation for these enzymes as putative novel drug targets. Although their therapeutic potential in an experimental model of VL has not been evaluated, it is advantageous that by targeting multiple intracellular enzymes, any compensation by functional orthologues would be blocked.

Table 1. Candidate proteins shortlisted based on maximum conservation among kinetoplastids subjected to BLAST analysis using the human homologs as query. Probable targets with least sequence similarity to the human homologs are listed. Highlights indicate the most divergent

Sl.No.	Selected Proteins from Table 1.	Acc. No.	e-value Human	% Identity	Human Acc. No.	Targetibility (Good/poor)	Organism in which studied with Ref.

sequences based on blast outcome.

1.	Leishmania donovani alpha tubulin (LDBPK_130330) mRNA, complete cds	>gi|398012101|ref|XM_003859197.1	0.0	82%	NP_116093.1	poor	*P. falciparum [71,72]* *T. brucei* [73]
2.	Leishmania donovani ATPase beta subunit, putative (LDBPK_251210) mRNA, complete cds	>gi|398016525|ref|XM_003861403.1	0.0	67%	NP_001677.2	poor	*T. brucei* [74] *L. donovani [75,76]* *P. falciparum* [77]
3.	Leishmania donovani casein kinase, putative (LDBPK_351030) mRNA, complete cds	>gi|398023052|ref|XM_003864640.1	2e-156	69%	NP_001885.1	poor	*T. brucei* [78]
4.	Leishmania donovani protein kinase, putative (LdBPK_280550.1) mRNA, complete cds	>gi|398017934|ref|XM_003862106.1	1e-76	44%	NP_003591.2	good	*T. brucei* [52,45] *P. falciparum* [15]
5.	Leishmania donovani serine/threonine protein phosphatase, putative (LDBPK_251360) mRNA, complete cds	>gi|398016555|ref|XM_003861418.1	5e-160	72%	NP_001009552.1	poor	*T. brucei* [79] *P. falciparum* [80-82]
6.	Leishmania donovani glutaredoxin, putative(LdBPK_201020.1) mRNA, complete cds	>gi|398014506|ref|XM_003860396.1	7e-09	34%	NP_001166984.1	good	*T. brucei* [83-85]
7.	Leishmania donovani fructose-1,6-bisphosphate aldolase (LDBPK_361320) mRNA, complete cds	>gi|398024173|ref|XM_003865200.1	9e-104	47%	NP_005156.1	good	*Trypanosoma* sp. [86] *P. falciparum* [87-88]
8.	Leishmania donovani adenosylhomocysteinase (LDBPK_364100.1) gene, complete cds	>gi|284794942|gb|GU353334.1	0.0	72%	NP_000678.1	poor	*T . cruzi* [89] *Others* [90-93]
9.	Leishmania donovani cell division related protein kinase 2 (LDBPK_360600) mRNA, complete cds	>gi|398024029|ref|XM_003865128.1	2e-126	60%	NP_001249.1	poor	
10.	Leishmania donovani DNA polymerase delta catalytic subunit, putative (LDBPK_331790) mRNA, complete cds	>gi|398021684|ref|XM_003863957.1	0.0	54%	NP_002682.2	average	*P. falciparum* [94]
11.	Leishmania donovani isolate MHOM/00/Khartoum LSB-52-1 pyruvate kinase gene, complete cds	>gi|154269431|gb|EU024521.1	1e-164	49%	NP_002645.3	good	*T. brucei* [95-96] *L. mexicana* [97]
12.	Leishmania donovani dihydrolipoamide dehydrogenase, putative (LDBPK_323510) mRNA, complete cds	>gi|398021197|ref|XM_003863714.1	2e-156	53%	NP_000099.2	average	*T. brucei* [98] *T. cruzi* [99]

Table 2. G-Score and hydrogen-bonded amino acid residues.

Ligands	**G-Score**	**H-bond with amino acid residue**
Hesperadin	-7.79	Asn 41, Phe 173
Barasertib	-7.28	Phe 173, Asn 121, Lys 60
GSK-1070916	-7.61	Gly 174

Reference

[1] P. Tsigankov, P.F. Gherardini, M. Helmer-Citterich, G.F. Spath, P.J. Myler, D. Zilberstein, Regulation dynamics of Leishmania differentiation: deconvoluting signals and identifying phosphorylation trends, Mol Cell Proteomics, 13 (2014) 1787-1799.
[2] M. Thiel, I. Bruchhaus, Comparative proteome analysis of Leishmania donovani at different stages of transformation from promastigotes to amastigotes, Med Microbiol Immunol, 190 (2001) 33-36.
[3] K. Leifso, G. Cohen-Freue, N. Dogra, A. Murray, W.R. McMaster, Genomic and proteomic expression analysis of Leishmania promastigote and amastigote life stages: the Leishmania genome is constitutively expressed, Mol Biochem Parasitol, 152 (2007) 35-46.
[4] M. Parsons, E.A. Worthey, P.N. Ward, J.C. Mottram, Comparative analysis of the kinomes of three pathogenic trypanosomatids: Leishmania major, Trypanosoma brucei and Trypanosoma cruzi, BMC Genomics, 6 (2005) 127.
[5] D. Fabbro, S.W. Cowan-Jacob, H. Mobitz, G. Martiny-Baron, Targeting cancer with small-molecular-weight kinase inhibitors, Methods Mol Biol, 795 (2012) 1-34.
[6] C. Doerig, Protein kinases as targets for anti-parasitic chemotherapy, Biochim Biophys Acta, 1697 (2004) 155-168.
[7] P. Salaun, Y. Rannou, C. Prigent, Cdk1, Plks, Auroras, and Neks: the mitotic bodyguards, Adv Exp Med Biol, 617 (2008) 41-56.
[8] B. Akiyoshi, K. Gull, Discovery of unconventional kinetochores in kinetoplastids, Cell, 156 (2014) 1247-1258.
[9] S. Monnerat, C.I. Almeida Costa, A.C. Forkert, C. Benz, A. Hamilton, L. Tetley, R. Burchmore, C. Novo, J.C. Mottram, T.C. Hammarton, Identification and Functional Characterisation of CRK12:CYC9, a Novel Cyclin-Dependent Kinase (CDK)-Cyclin Complex in Trypanosoma brucei, PLoS One, 8 (2013) e67327.
[10] T.C. Hammarton, S. Kramer, L. Tetley, M. Boshart, J.C. Mottram, Trypanosoma brucei Polo-like kinase is essential for basal body duplication, kDNA segregation and cytokinesis, Mol Microbiol, 65 (2007) 1229-1248.
[11] S.O. Ochiana, V. Pandarinath, Z. Wang, R. Kapoor, M.J. Ondrechen, L. Ruben, M.P. Pollastri, The human Aurora kinase inhibitor danusertib is a lead compound for anti-trypanosomal drug discovery via target repurposing, Eur J Med Chem, 62 (2013) 777-784.
[12] N.G. Jones, E.B. Thomas, E. Brown, N.J. Dickens, T.C. Hammarton, J.C. Mottram, Regulators of Trypanosoma brucei cell cycle progression and differentiation identified using a kinome-wide RNAi screen, PLoS Pathog, 10 (2014) e1003886.
[13] X. Tu, P. Kumar, Z. Li, C.C. Wang, An aurora kinase homologue is involved in regulating both mitosis and cytokinesis in Trypanosoma brucei, J Biol Chem, 281 (2006) 9677-9687.
[14] M.M. Siman-Tov, A.C. Ivens, C.L. Jaffe, Identification and cloning of Lmairk, a member of the Aurora/Ipl1p protein kinase family, from the human protozoan parasite Leishmania, Biochim Biophys Acta, 1519 (2001) 241-245.
[15] L. Reininger, J.M. Wilkes, H. Bourgade, D. Miranda-Saavedra, C. Doerig, An essential Aurora-related kinase transiently associates with spindle pole bodies during Plasmodium falciparum erythrocytic schizogony, Mol Microbiol, 79 (2011) 205-221.
[16] S. Li, Z. Deng, J. Fu, C. Xu, G. Xin, Z. Wu, J. Luo, G. Wang, S. Zhang, B. Zhang, F. Zou, Q. Jiang, C. Zhang, Spatial Compartmentalization Specializes the Function of Aurora A and Aurora B, J Biol Chem, 290 (2015) 17546-17558.
[17] T.G. Carvalho, C. Doerig, L. Reininger, Nima- and Aurora-related kinases of malaria parasites, Biochim Biophys Acta, 1834 (2013) 1336-1345.

[18] G. Patel, N.E. Roncal, P.J. Lee, S.E. Leed, J. Erath, A. Rodriguez, R.J. Sciotti, M.P. Pollastri, Repurposing human Aurora kinase inhibitors as leads for anti-protozoan drug discovery, Medchemcomm, 5 (2014) 655-658.
[19] P. Gavriilidis, A. Giakoustidis, D. Giakoustidis, Aurora Kinases and Potential Medical Applications of Aurora Kinase Inhibitors: A Review, J Clin Med Res, 7 (2015) 742-751.
[20] Y. Nakajima, R.G. Tyers, C.C. Wong, J.R. Yates, 3rd, D.G. Drubin, G. Barnes, Nbl1p: a Borealin/Dasra/CSC-1-like protein essential for Aurora/Ipl1 complex function and integrity in Saccharomyces cerevisiae, Mol Biol Cell, 20 (2009) 1772-1784.
[21] J.H. Kim, J.S. Kang, C.S. Chan, Sli15 associates with the ipl1 protein kinase to promote proper chromosome segregation in Saccharomyces cerevisiae, J Cell Biol, 145 (1999) 1381-1394.
[22] E.N. Pugacheva, S.A. Jablonski, T.R. Hartman, E.P. Henske, E.A. Golemis, HEF1-dependent Aurora A activation induces disassembly of the primary cilium, Cell, 129 (2007) 1351-1363.
[23] J. Pan, Q. Wang, W.J. Snell, An aurora kinase is essential for flagellar disassembly in Chlamydomonas, Dev Cell, 6 (2004) 445-451.
[24] Z. Li, C.C. Wang, Changing roles of aurora-B kinase in two life cycle stages of Trypanosoma brucei, Eukaryot Cell, 5 (2006) 1026-1035.
[25] Z. Li, J.H. Lee, F. Chu, A.L. Burlingame, A. Gunzl, C.C. Wang, Identification of a novel chromosomal passenger complex and its unique localization during cytokinesis in Trypanosoma brucei, PLoS One, 3 (2008) e2354.
[26] A.M. Waterhouse, J.B. Procter, D.M. Martin, M. Clamp, G.J. Barton, Jalview Version 2--a multiple sequence alignment editor and analysis workbench, Bioinformatics, 25 (2009) 1189-1191.
[27] K. Tamura, G. Stecher, D. Peterson, A. Filipski, S. Kumar, MEGA6: Molecular Evolutionary Genetics Analysis version 6.0, Mol Biol Evol, 30 (2013) 2725-2729.
[28] O.H. Lowry, N.J. Rosebrough, A.L. Farr, R.J. Randall, Protein measurement with the Folin phenol reagent, J Biol Chem, 193 (1951) 265-275.
[29] W. Wray, T. Boulikas, V.P. Wray, R. Hancock, Silver staining of proteins in polyacrylamide gels, Anal Biochem, 118 (1981) 197-203.
[30] S. Bhowmick, N. Ali, Identification of novel Leishmania donovani antigens that help define correlates of vaccine-mediated protection in visceral leishmaniasis, PLoS One, 4 (2009) e5820.
[31] H.M. Cooper, Y. Paterson, Production of polyclonal antisera, Curr Protoc Neurosci, Chapter 5 (2009) Unit 5 5.
[32] N.J. Greenfield, Using circular dichroism spectra to estimate protein secondary structure, Nat Protoc, 1 (2006) 2876-2890.
[33] C. Louis-Jeune, M.A. Andrade-Navarro, C. Perez-Iratxeta, Prediction of protein secondary structure from circular dichroism using theoretically derived spectra, Proteins, 80 (2012) 374-381.
[34] N. Eswar, B. Webb, M.A. Marti-Renom, M.S. Madhusudhan, D. Eramian, M.Y. Shen, U. Pieper, A. Sali, Comparative protein structure modeling using Modeller, Curr Protoc Bioinformatics, Chapter 5 (2006) Unit 5 6.
[35] E.F. Pettersen, T.D. Goddard, C.C. Huang, G.S. Couch, D.M. Greenblatt, E.C. Meng, T.E. Ferrin, UCSF Chimera--a visualization system for exploratory research and analysis, J Comput Chem, 25 (2004) 1605-1612.
[36] T. Halgren, New method for fast and accurate binding-site identification and analysis, Chem Biol Drug Des, 69 (2007) 146-148.
[37] T.A. Halgren, R.B. Murphy, R.A. Friesner, H.S. Beard, L.L. Frye, W.T. Pollard, J.L. Banks, Glide: a new approach for rapid, accurate docking and scoring. 2. Enrichment factors in database screening, J Med Chem, 47 (2004) 1750-1759.
[38] F. Afrin, N. Ali, Adjuvanticity and protective immunity elicited by Leishmania donovani antigens encapsulated in positively charged liposomes, Infect Immun, 65 (1997) 2371-2377.

[39] S. Goyard, H. Segawa, J. Gordon, M. Showalter, R. Duncan, S.J. Turco, S.M. Beverley, An in vitro system for developmental and genetic studies of Leishmania donovani phosphoglycans, Mol Biochem Parasitol, 130 (2003) 31-42.
[40] A.L. Fulwiler, D.R. Soysa, B. Ullman, P.A. Yates, A rapid, efficient and economical method for generating leishmanial gene targeting constructs, Mol Biochem Parasitol, 175 (2011) 209-212.
[41] K.A. Robinson, S.M. Beverley, Improvements in transfection efficiency and tests of RNA interference (RNAi) approaches in the protozoan parasite Leishmania, Mol Biochem Parasitol, 128 (2003) 217-228.
[42] G. Juan, E. Hernando, C. Cordon-Cardo, Separation of live cells in different phases of the cell cycle for gene expression analysis, Cytometry, 49 (2002) 170-175.
[43] J. Achilles, F. Stahl, H. Harms, S. Muller, Isolation of intact RNA from cytometrically sorted Saccharomyces cerevisiae for the analysis of intrapopulation diversity of gene expression, Nat Protoc, 2 (2007) 2203-2211.
[44] M.W. Pfaffl, A new mathematical model for relative quantification in real-time RT-PCR, Nucleic Acids Res, 29 (2001) e45.
[45] N. Jetton, K.G. Rothberg, J.G. Hubbard, J. Wise, Y. Li, H.L. Ball, L. Ruben, The cell cycle as a therapeutic target against Trypanosoma brucei: Hesperadin inhibits Aurora kinase-1 and blocks mitotic progression in bloodstream forms, Mol Microbiol, 72 (2009) 442-458.
[46] Z.L. Wu, Phosphatase-coupled universal kinase assay and kinetics for first-order-rate coupling reaction, PLoS One, 6 (2011) e23172.
[47] J. Mikus, D. Steverding, A simple colorimetric method to screen drug cytotoxicity against Leishmania using the dye Alamar Blue, Parasitol Int, 48 (2000) 265-269.
[48] M. Carmena, W.C. Earnshaw, The cellular geography of aurora kinases, Nat Rev Mol Cell Biol, 4 (2003) 842-854.
[49] N. Minocha, D. Kumar, K. Rajanala, S. Saha, Kinetoplast morphology and segregation pattern as a marker for cell cycle progression in Leishmania donovani, J Eukaryot Microbiol, 58 (2011) 249-253.
[50] A. Pigula, D.G. Drubin, G. Barnes, Regulation of mitotic spindle disassembly by an environmental stress-sensing pathway in budding yeast, Genetics, 198 (2014) 1043-1057.
[51] D. Kachaner, X. Pinson, K.B. El Kadhi, K. Normandin, L. Talje, H. Lavoie, G. Lepine, S. Carreno, B.H. Kwok, G.R. Hickson, V. Archambault, Interdomain allosteric regulation of Polo kinase by Aurora B and Map205 is required for cytokinesis, J Cell Biol, 207 (2014) 201-211.
[52] Z. Li, T. Umeyama, C.C. Wang, The Aurora Kinase in Trypanosoma brucei plays distinctive roles in metaphase-anaphase transition and cytokinetic initiation, PLoS Pathog, 5 (2009) e1000575.
[53] R. Crane, B. Gadea, L. Littlepage, H. Wu, J.V. Ruderman, Aurora A, meiosis and mitosis, Biol Cell, 96 (2004) 215-229.
[54] J.R. Bischoff, L. Anderson, Y. Zhu, K. Mossie, L. Ng, B. Souza, B. Schryver, P. Flanagan, F. Clairvoyant, C. Ginther, C.S. Chan, M. Novotny, D.J. Slamon, G.D. Plowman, A homologue of Drosophila aurora kinase is oncogenic and amplified in human colorectal cancers, EMBO J, 17 (1998) 3052-3065.
[55] D. Demidov, I. Lermontova, O. Weiss, J. Fuchs, T. Rutten, K. Kumke, T.F. Sharbel, D. Van Damme, N. De Storme, D. Geelen, A. Houben, Altered expression of Aurora kinases in Arabidopsis results in aneu- and polyploidization, Plant J, 80 (2014) 449-461.
[56] E. Hannak, M. Kirkham, A.A. Hyman, K. Oegema, Aurora-A kinase is required for centrosome maturation in Caenorhabditis elegans, J Cell Biol, 155 (2001) 1109-1116.
[57] T. Marumoto, S. Honda, T. Hara, M. Nitta, T. Hirota, E. Kohmura, H. Saya, Aurora-A kinase maintains the fidelity of early and late mitotic events in HeLa cells, J Biol Chem, 278 (2003) 51786-51795.
[58] S.J. Radford, J.K. Jang, K.S. McKim, The chromosomal passenger complex is required for meiotic acentrosomal spindle assembly and chromosome biorientation, Genetics, 192 (2012) 417-429.

[59] R. Giet, D.M. Glover, Drosophila aurora B kinase is required for histone H3 phosphorylation and condensin recruitment during chromosome condensation and to organize the central spindle during cytokinesis, J Cell Biol, 152 (2001) 669-682.
[60] Y. Terada, M. Tatsuka, F. Suzuki, Y. Yasuda, S. Fujita, M. Otsu, AIM-1: a mammalian midbody-associated protein required for cytokinesis, EMBO J, 17 (1998) 667-676.
[61] S. Hauf, R.W. Cole, S. LaTerra, C. Zimmer, G. Schnapp, R. Walter, A. Heckel, J. van Meel, C.L. Rieder, J.M. Peters, The small molecule Hesperadin reveals a role for Aurora B in correcting kinetochore-microtubule attachment and in maintaining the spindle assembly checkpoint, J Cell Biol, 161 (2003) 281-294.
[62] H. Hochegger, N. Hegarat, J.B. Pereira-Leal, Aurora at the pole and equator: overlapping functions of Aurora kinases in the mitotic spindle, Open Biol, 3 (2013) 120185.
[63] E.O. Johnson, K.H. Chang, Y. de Pablo, S. Ghosh, R. Mehta, S. Badve, K. Shah, PHLDA1 is a crucial negative regulator and effector of Aurora A kinase in breast cancer, J Cell Sci, 124 (2011) 2711-2722.
[64] R. Ban, T. Nishida, T. Urano, Mitotic kinase Aurora-B is regulated by SUMO-2/3 conjugation/deconjugation during mitosis, Genes Cells, 16 (2011) 652-669.
[65] C. Naula, M. Parsons, J.C. Mottram, Protein kinases as drug targets in trypanosomes and Leishmania, Biochim Biophys Acta, 1754 (2005) 151-159.
[66] M. Vieth, R.E. Higgs, D.H. Robertson, M. Shapiro, E.A. Gragg, H. Hemmerle, Kinomics-structural biology and chemogenomics of kinase inhibitors and targets, Biochim Biophys Acta, 1697 (2004) 243-257.
[67] F. Sessa, F. Villa, Structure of Aurora B-INCENP in complex with barasertib reveals a potential transinhibitory mechanism, Acta Crystallogr F Struct Biol Commun, 70 (2014) 294-298.
[68] F. Shamsipour, S. Hosseinzadeh, S.S. Arab, S. Vafaei, S. Farid, M. Jeddi-Tehrani, S. Balalaie, Synthesis and investigation of new Hesperadin analogues antitumor effects on HeLa cells, J Chem Biol, 7 (2014) 85-91.
[69] B. Zhang, Y. Li, H. Zhang, C. Ai, 3D-QSAR and molecular docking studies on derivatives of MK-0457, GSK1070916 and SNS-314 as inhibitors against Aurora B kinase, Int J Mol Sci, 11 (2010) 4326-4347.
[70] G.J. Crowther, D. Shanmugam, S.J. Carmona, M.A. Doyle, C. Hertz-Fowler, M. Berriman, S. Nwaka, S.A. Ralph, D.S. Roos, W.C. Van Voorhis, F. Aguero, Identification of attractive drug targets in neglected-disease pathogens using an in silico approach, PLoS Negl Trop Dis, 4 (2010) e804.
[71] B.J. Fennell, Z.A. Al-shatr, A. Bell, Isotype expression, post-translational modification and stage-dependent production of tubulins in erythrocytic Plasmodium falciparum, Int J Parasitol, 38 (2008) 527-539.
[72] T.W. Kooij, B. Franke-Fayard, J. Renz, H. Kroeze, M.W. van Dooren, J. Ramesar, K.D. Augustijn, C.J. Janse, A.P. Waters, Plasmodium berghei alpha-tubulin II: a role in both male gamete formation and asexual blood stages, Mol Biochem Parasitol, 144 (2005) 16-26.
[73] P.G. McKean, A. Baines, S. Vaughan, K. Gull, Gamma-tubulin functions in the nucleation of a discrete subset of microtubules in the eukaryotic flagellum, Curr Biol, 13 (2003) 598-602.
[74] A. Schnaufer, G.D. Clark-Walker, A.G. Steinberg, K. Stuart, The F1-ATP synthase complex in bloodstream stage trypanosomes has an unusual and essential function, EMBO J, 24 (2005) 4029-4040.
[75] D. Mandal, T. Mukherjee, S. Sarkar, S. Majumdar, A. Bhaduri, The plasma-membrane Ca2+-ATPase of Leishmania donovani is an extrusion pump for Ca2+, Biochem J, 322 (Pt 1) (1997) 251-257.
[76] A. Das, Studies on mitochondrial ATPase of Leishmania donovani using digitonin-permeabilized promastigotes, Mol Biochem Parasitol, 60 (1993) 293-301.
[77] M. Ahmad, S. Singh, F. Afrin, R. Tuteja, Novel RuvB nuclear ATPase is specific to intraerythrocytic mitosis during schizogony of Plasmodium falciparum, Mol Biochem Parasitol, 185 (2012) 58-65.
[78] M.D. Urbaniak, Casein kinase 1 isoform 2 is essential for bloodstream form Trypanosoma brucei, Mol Biochem Parasitol, 166 (2009) 183-185.

[79] M. Chaudhuri, Cloning and characterization of a novel serine/threonine protein phosphatase type 5 from Trypanosoma brucei, Gene, 266 (2001) 1-13.
[80] R. Kumar, B. Adams, A. Oldenburg, A. Musiyenko, S. Barik, Characterisation and expression of a PP1 serine/threonine protein phosphatase (PfPP1) from the malaria parasite, Plasmodium falciparum: demonstration of its essential role using RNA interference, Malar J, 1 (2002) 5.
[81] S. Dobson, V. Bracchi, D. Chakrabarti, S. Barik, Characterization of a novel serine/threonine protein phosphatase (PfPPJ) from the malaria parasite, Plasmodium falciparum, Mol Biochem Parasitol, 115 (2001) 29-39.
[82] D. Yokoyama, A. Saito-Ito, N. Asao, K. Tanabe, M. Yamamoto, T. Matsumura, Modulation of the growth of Plasmodium falciparum in vitro by protein serine/threonine phosphatase inhibitors, Biochem Biophys Res Commun, 247 (1998) 18-23.
[83] B. Manta, C. Pavan, M. Sturlese, A. Medeiros, M. Crispo, C. Berndt, R.L. Krauth-Siegel, M. Bellanda, M.A. Comini, Iron-sulfur cluster binding by mitochondrial monothiol glutaredoxin-1 of Trypanosoma brucei: molecular basis of iron-sulfur cluster coordination and relevance for parasite infectivity, Antioxid Redox Signal, 19 (2013) 665-682.
[84] S. Ceylan, V. Seidel, N. Ziebart, C. Berndt, N. Dirdjaja, R.L. Krauth-Siegel, The dithiol glutaredoxins of african trypanosomes have distinct roles and are closely linked to the unique trypanothione metabolism, J Biol Chem, 285 (2010) 35224-35237.
[85] M.A. Comini, J. Rettig, N. Dirdjaja, E.M. Hanschmann, C. Berndt, R.L. Krauth-Siegel, Monothiol glutaredoxin-1 is an essential iron-sulfur protein in the mitochondrion of African trypanosomes, J Biol Chem, 283 (2008) 27785-27798.
[86] J. Perie, I. Riviere-Alric, C. Blonski, T. Gefflaut, N. Lauth de Viguerie, M. Trinquier, M. Willson, F.R. Opperdoes, M. Callens, Inhibition of the glycolytic enzymes in the trypanosome: an approach in the development of new leads in the therapy of parasitic diseases, Pharmacol Ther, 60 (1993) 347-365.
[87] C.A. Buscaglia, W.G. Hol, V. Nussenzweig, T. Cardozo, Modeling the interaction between aldolase and the thrombospondin-related anonymous protein, a key connection of the malaria parasite invasion machinery, Proteins, 66 (2007) 528-537.
[88] U. Certa, P. Ghersa, H. Dobeli, H. Matile, H.P. Kocher, I.K. Shrivastava, A.R. Shaw, L.H. Perrin, Aldolase activity of a Plasmodium falciparum protein with protective properties, Science, 240 (1988) 1036-1038.
[89] Q.S. Li, S. Cai, J. Fang, R.T. Borchardt, K. Kuczera, C.R. Middaugh, R.L. Schowen, Evaluation of NAD(H) analogues as selective inhibitors for Trypanosoma cruzi S-adenosylhomocysteine hydrolase, Nucleosides Nucleotides Nucleic Acids, 28 (2009) 473-484.
[90] M. Nakanishi, [S-adenosyl-L-homocysteine hydrolase as an attractive target for antimicrobial drugs], Yakugaku Zasshi, 127 (2007) 977-982.
[91] H.R. Moon, K.M. Lee, J.H. Lee, S.K. Lee, S.B. Park, M.W. Chun, L.S. Jeong, Structure-activity relationship of 5'-substituted fluoro-neplanocin a analogues as potent inhibitors of S-adenosylhomocysteine hydrolase, Nucleosides Nucleotides Nucleic Acids, 24 (2005) 707-708.
[92] H.R. Moon, H.J. Lee, K.R. Kim, K.M. Lee, S.K. Lee, H.O. Kim, M.W. Chun, L.S. Jeong, Synthesis of 5'-substituted fluoro-neplanocin A analogues: importance of a hydrogen bonding donor at 5'-position for the inhibitory activity of S-adenosylhomocysteine hydrolase, Bioorg Med Chem Lett, 14 (2004) 5641-5644.
[93] Y. Huang, J. Komoto, Y. Takata, D.R. Powell, T. Gomi, H. Ogawa, M. Fujioka, F. Takusagawa, Inhibition of S-adenosylhomocysteine hydrolase by acyclic sugar adenosine analogue D-eritadenine. Crystal structure of S-adenosylhomocysteine hydrolase complexed with D-eritadenine, J Biol Chem, 277 (2002) 7477-7482.
[94] U. Bachrach, L. Abu-Elheiga, Effect of polyamines on the activity of malarial alpha-like DNA polymerase, Eur J Biochem, 191 (1990) 633-637.

[95] M. Callens, D.A. Kuntz, F.R. Opperdoes, Characterization of pyruvate kinase of Trypanosoma brucei and its role in the regulation of carbohydrate metabolism, Mol Biochem Parasitol, 47 (1991) 19-29.
[96] I.W. Flynn, I.B. Bowman, Some kinetic properties of pyruvate kinase from Trypanosoma brucei: influence of pH and fructose-1,6-diphosphate, Mol Biochem Parasitol, 4 (1981) 95-106.
[97] H.P. Morgan, I.W. McNae, M.W. Nowicki, V. Hannaert, P.A. Michels, L.A. Fothergill-Gilmore, M.D. Walkinshaw, Allosteric mechanism of pyruvate kinase from Leishmania mexicana uses a rock and lock model, J Biol Chem, 285 (2010) 12892-12898.
[98] A. Roldan, M.A. Comini, M. Crispo, R.L. Krauth-Siegel, Lipoamide dehydrogenase is essential for both bloodstream and procyclic Trypanosoma brucei, Mol Microbiol, 81 (2011) 623-639.
[99] J. Gutierrez-Correa, Trypanosoma cruzi dihydrolipoamide dehydrogenase as target for phenothiazine cationic radicals. Effect of antioxidants, Curr Drug Targets, 7 (2006) 1155-1179.

CONFLICT OF INTEREST

The authors declare that they have no conflicts of interest with the contents of this article.

AUTHOR CONTRIBUTIONS

NA designed, analyzed, critically revised and approved the final version to be published. RC designed, performed and analyzed the experiments, prepared the figures and wrote the paper. AB performed the cell sorting and immunoblot experiments. PP and ND performed the docking studies. ND and SM performed experiments on transfection and macrophage attachment respectively. All authors analyzed the results and approved the final version of the manuscript.

ACKNOWLEDGEMENTS

The authors are grateful to Dr. A. Dube, CDRI, Lucknow for gifting the recombinant *L donovani* H3 clone, to Dr. P. Yates, OHSU for help in the creation of the knock-out constructs, to Tanmoy Dalui, CSIR-IICB and Debajit Bhowmick, CRNN, CU for help with FACS experiments, Dr. S. Chakraborty, CSIR-IICB for bioinformatic analyses and to Mohd Shameel Iqbal, Mohammad Asad and Mithun Maji for discussions.

FOOTNOTES

This work was supported by grants from CSIR, New Delhi to RC, a CSIR-Senior Research Fellow (No. 31/002(0854)/2010/EMR-I). AB, ND (UGC) and SM thank CSIR for fellowship-(No. 13(97)/13/NA-NA/381/(NWP); No. Admn. 13 (45)/2013/JRF (UGC) and No.Admn-1(9)/2010/JRF (CSIR). ND and PP were recipients of fellowship from a DST funded project (Ref. No. SB/FT/LS-269/2012).

ABBREVIATIONS

VL- Visceral Leishmaniasis

Figure 1. Sequence comparison and domain organization of putative Ld*AIRK*.

(**A**) Multiple sequence alignment of amino acid sequences performed using ClustalW and visualized using Jalview 2.8 comparing Aurora kinase homologs from *H. sapiens, T. brucei, T. cruzi, L. donovani, L. major, L. mexicana and L. braziliensis*. Conserved residues are shown by the purple background with the colour intensity increasing as conservation increases. The numbers at the left and right indicate amino acid positions. (**B**) Sequence based map depicting the typical domains and their conserved regions of all aligned Aurora kinases. The ATP binding site, activation loop and destruction box regions are boxed and highlighted in green, pink and yellow respectively.

Figure 2. Cell-cycle-regulated sub-cellular localization of LdAIRK.

(**A**) Bright field (BF) image of 5 days infected mouse peritoneal macrophage immunostained with FITC tagged antibody against LdAIRK (*left)* and DAPI nuclear stain (*middle*) with their merged images *(right)*.A diffuse ring of cytosolic localization outside each amastigote nuclear region is observed. (**B**) Representative promastigotes of each cell-cycle phase, with their bright field images *(extreme left)* immunostained with the antibody against LdAIRK (*left)* and DAPI nuclear stain (*middle*) with their merged images *(right)*. Cells were analyzed by confocal microscopy and the images are representative of three independent preparations. The inserted box represents 2.5× zoom of the merged image. *N*, nucleus; *K*, kinetoplast. *Scale bar,* 10μm.

Figure 3. Cell-cycle-regulated expression of LdAIRK.

(**A**) Total cellular RNA from cells of each phase, subjected to RT-PCR using primers for a 300 bp region of LdAIRK. The mRNA levels were normalized to a 300 bp LdGAPDH amplicon used as the housekeeping control. G1 cells were used as the reference control. Asterisks above bars indicate significant difference compared with reference control (*$p< 0.05$, **$p< 0.01$). The results are representative of three independent experiments. (**B**) Whole-cell lysate of each phase subjected to immunoblot analysis and probed with anti-LdAIRK antibody. The LdAIRK levels were normalised to LdActin levels. G1 cells were used as the reference control. Asterisks above bars in the *lower panel*,(plot of band intensity as created by densitometric analysis using ImageJ software) indicate significant difference compared with reference control. (*$p< 0.05$,**$p< 0.01$). The results are representative of three independent experiments.

Figure 4. *In vitro* kinetic analysis of LdAIRK.

(**A**) A radioactive *in vitro* kinase assay with LdH3 as substrate depicts the presence of kinase activity in recombinant $(His)_6$-LdAIRK. The band at 35kDa and 26kDa shows auto-phosphorylation activity in addition to LdH3 phosphorylation seen at 20kDa position. The reactions were resolved on SDS-PAGE followed by Coomassie Blue staining (Coomassie) and autoradiography of the same gel (Autoradiogram). (**B**) Michaelis–Menten and Lineweaver-Burk plot (inlet) to determine the K_M and V_{MAX} for ATP at saturating LdH3 conditions. The data at

ATP concentrations (0-200µM) and time points (0-120 seconds) were analyzed by non-linear regression using Prism5 (GraphPad Software Inc.). Data given are representative of three experiments. (**C**) Nucleotide preference of LdAIRK as determined by nucleotide completion assay (1mM each of unlabelled ATP/GTP/CTP/TTP). Only unlabeled ATP prevented phosphorylation of LdH3.

Figure 5. Ligand docking and *in vitro* dose-response evaluation of kinase activity.

(**A**) Molecular structures of different ligands (Hesperadin, GSK-1070916, Barasertib) and their GLIDE docking images with Ld*AIRK* depicting their interaction with active-site residues. The H-bond lengths are depicted in yellow. (**B**) Dose–response upon inhibition of LdAIRK by Hesperadin, GSK-1070916 and Barasertib. The *upper panel* shows an autoradiograph of ^{32}P incorporated into LdH3 with corresponding Coomassie stained gels to check for equal loading of substrate LdH3. Densitometric analysis of the bands was performed using ImageJ software (NIH), and the percentage activity was plotted against Log_{10}[Ligand concentration] to calculate the IC50 (*lower panel)*. Data given are representative of three independent experiments.

Figure 6. Effect of LdAIRK inhibition on parasite viability.

(**A**) A plot of % survivability of amastigotes upon treatment with different drug concentrations for 72 hours, enumerated by analysis of Giemsa stained coverslips. Bars represent means ± SEM of three independent experiments (n=200 each time). (**B**) Dose-response curve of promastigote growth obtained upon incubation of log-phase promastigotes with different concentrations of inhibitors for different time points (24 h, 48 h or 72h). The data points were generated based on Alamar blue reduction assay and IC50 values determined. Data given are representative of three independent experiments performed in duplicate.

Figure 7. Effect of LdAIRK inhibition on cell-cycle progression.

(**A**) Time samples of IC50 dose treated promastigotes were collected, stained with propidium iodide and analyzed by FACS for DNA content. Time points (0h, 24h, 48h, 72h) and ploidy of peaks (2C, 4C, 6C, 8C) are indicated. The histograms are a representative image of three independent experiments (**B**) The percentage of cells in sub$G_{0,}$ G1, S, G2/M phases or beyond as determined by the FACSDiva software are plotted graphically. The percentages represent the means of all the three independent experiments.

Figure 8. Effect of LdAIRK inhibition on parasite morphology and nuclear phenotype.

(**A**) Merged DAPI stained and brightfield images of parasites after treatment for varying time-points (0h, 24h, 48h, 72h).The images are representative of three independent slide preparations. (**B**) Graphical representation depicting the nucleus and kinetoplast configurations of Hesperadin-treated and untreated parasites. The percentages are representative of 200 cells per time point. *N*, nucleus; *K*, kinetoplast. *Scale bar,* 10µm.

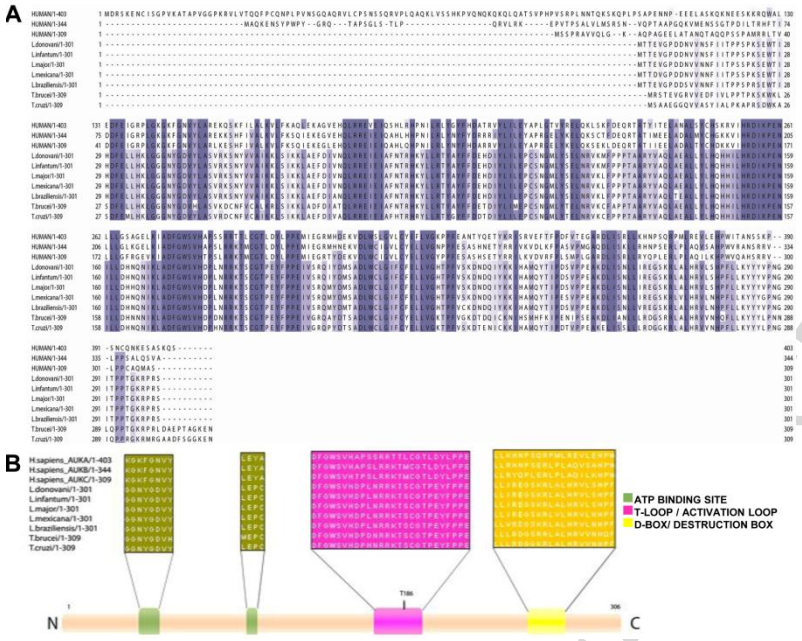

Fig. 1

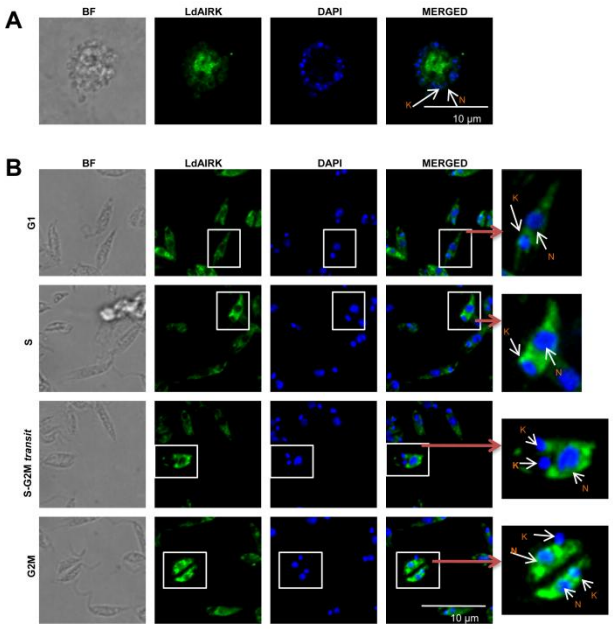

Fig. 2

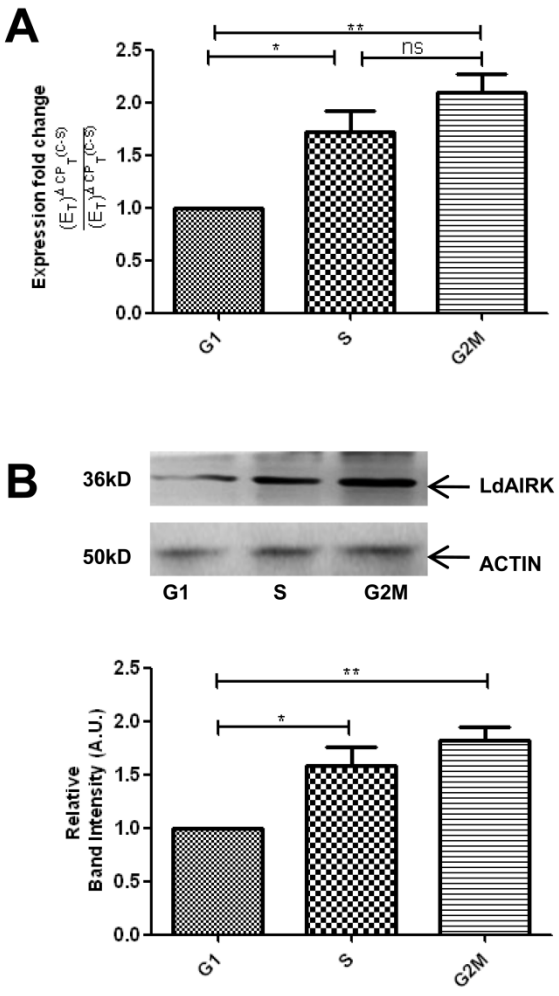

Fig. 3

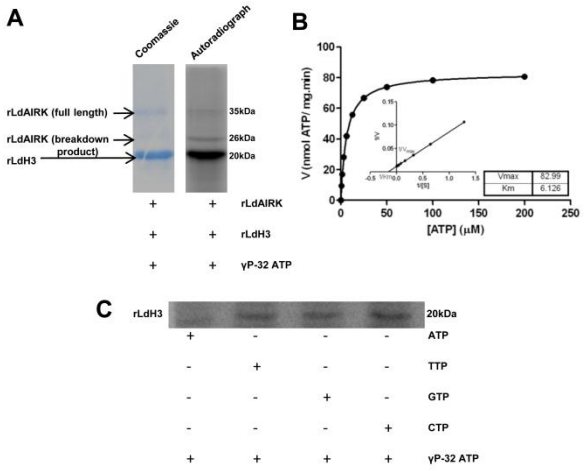

Fig. 4

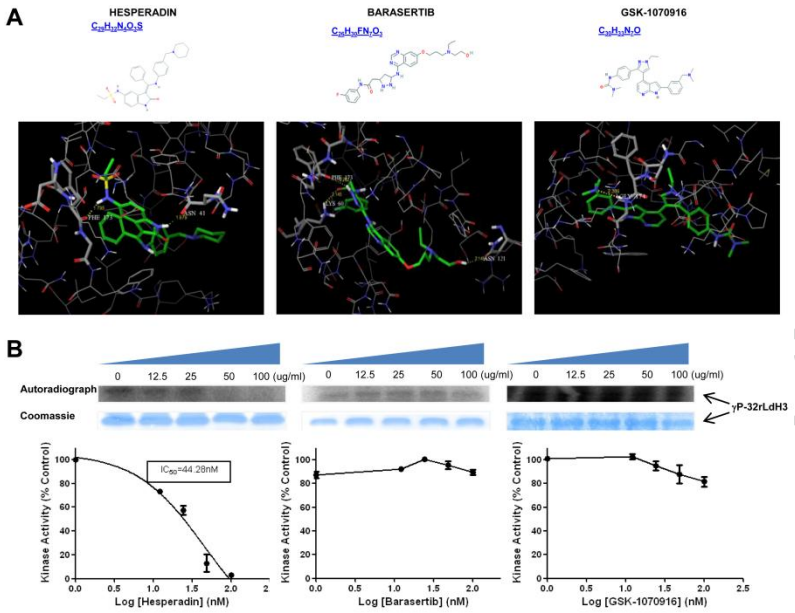

Fig. 5

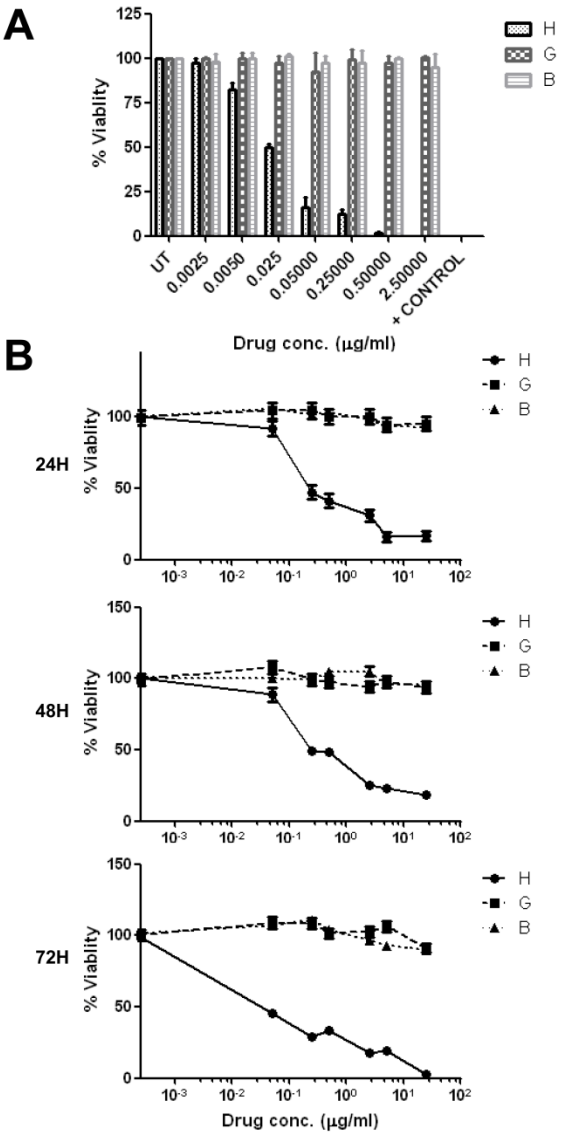

Fig. 6

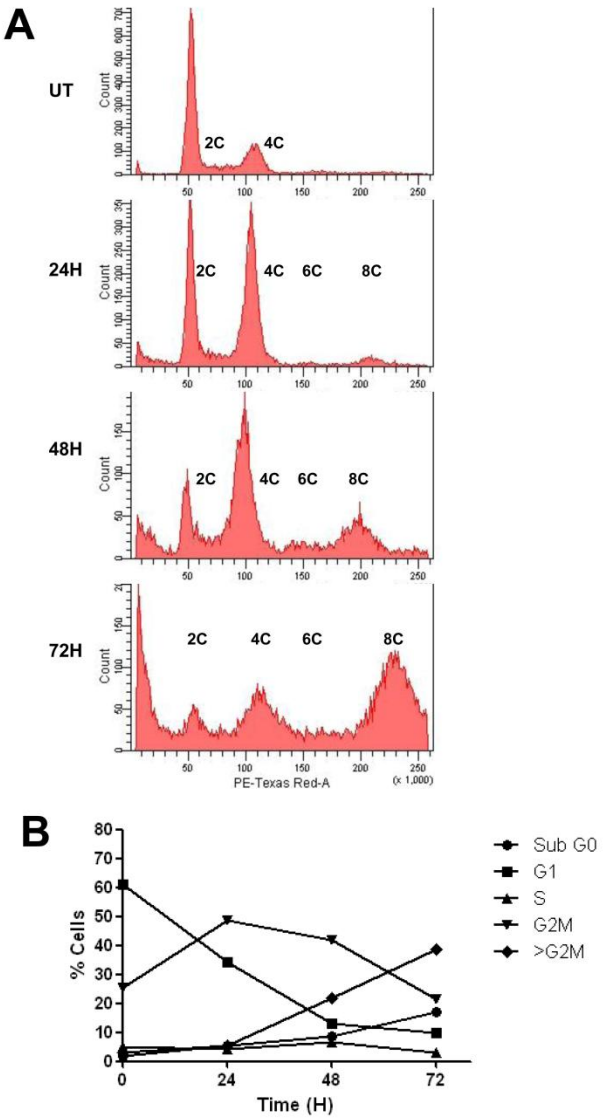

Fig. 7

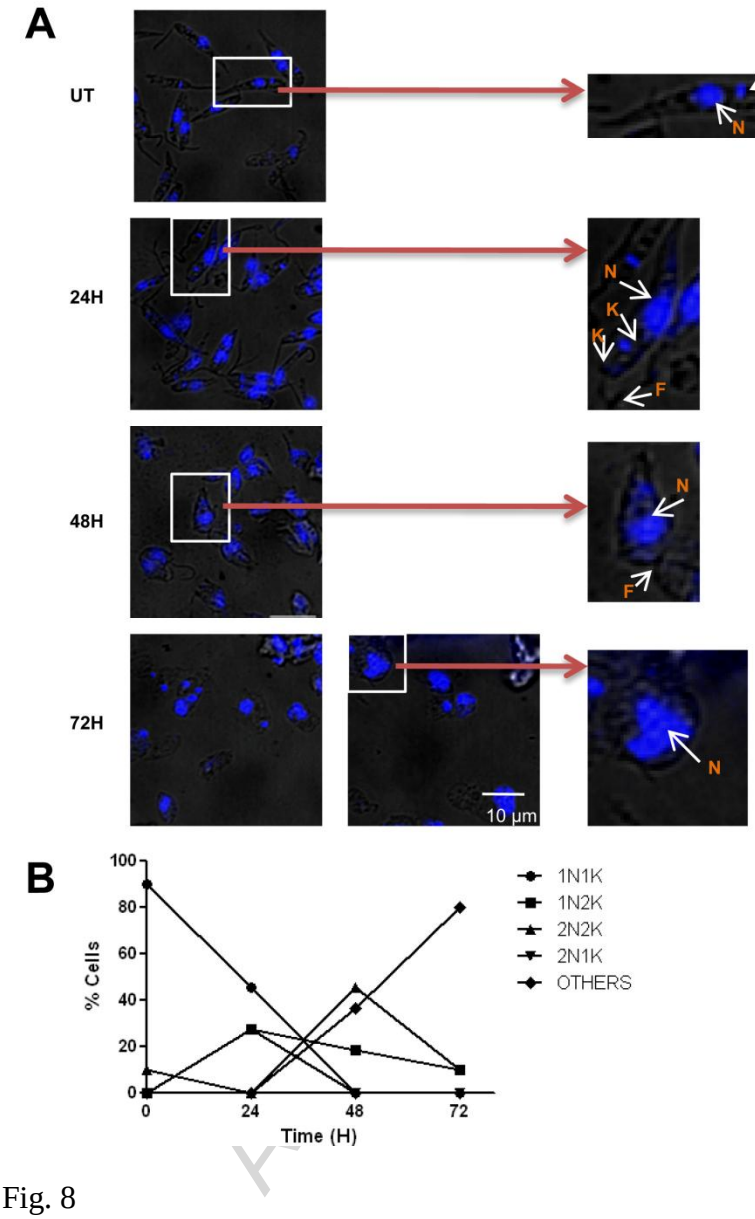

Fig. 8

HIGHLIGHTS:

1. An *L. donovani* Aurora kinase with properties of both aurora A and B is researched
2. Mammalian aurora inhibitors tested for anti-parasitic activity- Target Repurposing
3. A common lead against malaria, trypanosomiasis and leishmaniasis established
4. A role for LdAIRK in cell-cycle progression implicated – mitosis and cytokinesis.
5. LdAIRK proposed as a therapeutic target against VL.